

Original Article

Cite this article: Graziani R, Montomoli C, Iaccarino S, Menegon L, Nania L, and Carosi R (2020) Structural setting of a transpressive shear zone: insights from geological mapping, quartz petrofabric and kinematic vorticity analysis in NE Sardinia (Italy). *Geological Magazine* **157**: 1898–1916. <https://doi.org/10.1017/S0016756820000138>

Received: 17 October 2019

Revised: 3 January 2020

Accepted: 2 February 2020

First published online: 20 April 2020

Keywords:


transpressional tectonics; vorticity of flow; quartz crystallographic preferred orientation; EBSD; Variscan Belt; Sardinia

Author for correspondence:

Chiara Montomoli,

Email: chiara.montomoli@unito.it

Structural setting of a transpressive shear zone: insights from geological mapping, quartz petrofabric and kinematic vorticity analysis in NE Sardinia (Italy)

Riccardo Graziani¹, Chiara Montomoli^{2,3} , Salvatore Iaccarino², Luca Menegon^{4,5}, Laura Nania^{6,7} and Rodolfo Carosi²

¹Earth and Environmental Sciences, IKBSAS, University of British Columbia Okanagan, 3333 University Way, Kelowna, BC V1V 1V7, Canada; ²Dipartimento di Scienze della Terra, Università di Torino, via Valperga Caluso 35, 10125, Torino, Italy; ³IGG-CNR via Moruzzi 6, Pisa, Italy; ⁴The Njord Centre, Department of Geosciences, University of Oslo, P.O. Box 1048 Blindern, Norway; ⁵School of Geography, Earth and Environmental Sciences, Plymouth University, Plymouth PL4 8AA, UK; ⁶Dottorato Regionale in Scienze della Terra Pegaso, Università di Firenze, via La Pira 4, 50121, Firenze, Italy and ⁷Dipartimento di Scienze della Terra, Università di Pisa, via Santa Maria, 53, 56126, Pisa, Italy

Abstract

The Posada–Asinara Line is a crustal-scale transpressive shear zone affecting the Variscan basement in northern Sardinia during Late Carboniferous time. We investigated a structural transect of the Posada–Asinara Line (Baronie) with the aid of geological mapping and structural analysis. N-verging F2 isoclinal folds with associated mylonitic foliation (S2) are the main deformation features developed during the Posada–Asinara Line activity (D2). The mineral assemblages and microstructures suggest that the Posada–Asinara Line was affected by a retrograde metamorphic path. This is also confirmed by quartz microstructures, where subgrain rotation recrystallization superimposes on grain boundary migration recrystallization. Crystallographic preferred orientation data, obtained using electron backscatter diffraction, allowed analysis of quartz slip systems and estimation of the deformation temperature, vorticity of flow and rheological parameters (flow stress and strain rate) during the Posada–Asinara Line activity. Quartz deformation temperatures of 400 ± 50 °C have been estimated along a transect perpendicular to the Posada–Asinara Line, in agreement with the syn-kinematic post-metamorphic peak mineral assemblages and the late microstructures of quartz. The D2 phase can be subdivided in two events: an early D2_{early} phase, related to the metamorphic peak and low kinematic vorticity (pure shear dominated), and a late D2_{late} phase characterized by a lower metamorphic grade and an increased kinematic vorticity (simple shear dominated). Palaeopiezometry and strain rate estimates associated with the D2_{late} deformation event showed an intensity gradient increasing towards the core of the shear zone. The D2_{early} deformation developed under peak temperature conditions, while the D2_{late} event was active at shallower structural levels.

1. Introduction

Collisional type orogens are often characterized by the presence of crustal-scale shear zones driving and affecting the tectono-metamorphic evolution of the inner portion of the belts (Fossen & Cavalcante, 2017). Such crustal-scale shear zones can show different kinematics, from normal-sense (e.g. South Tibetan Detachment System; Burchfiel *et al.* 1992) to thrust-sense (e.g. Main Central Thrust; Searle *et al.* 2008 and Higher Himalayan Discontinuity; Montomoli *et al.* 2013, 2015) up to tension and transpression (Goscombe *et al.* 2005). Regardless, their long-lasting tectonic history (several Ma) is able to have a deep impact on the *P–T–t* paths of the metamorphic rocks and their exhumation (Carosi *et al.* 2018 and references therein).

Transpressive tectonics, at the regional scale, can result from different factors such as an oblique convergence (e.g. Coast Mountains; Depine *et al.* 2011) or the irregular shape of the continental margins (e.g. Armorican Massif; Gébelin *et al.* 2009). Regardless, the occurrence of transpression coeval with or subsequent to the continental collision deeply affects the evolution of the orogen with respect to the frontal collisional setting.

During the last 30 years, many theoretical, modelling and fieldwork studies have been carried out in order to characterize transpressional tectonics in complex oblique collisional events (e.g. Sanderson & Marchini, 1984; Tikoff & Fossen, 1993; Tikoff & Teyssier, 1994; Fossen & Tikoff, 1998; Schulmann *et al.* 2003). Occurrences of transpressional tectonics are often related to collisional belts where transpression represents an evolution of the nappe stacking and crustal

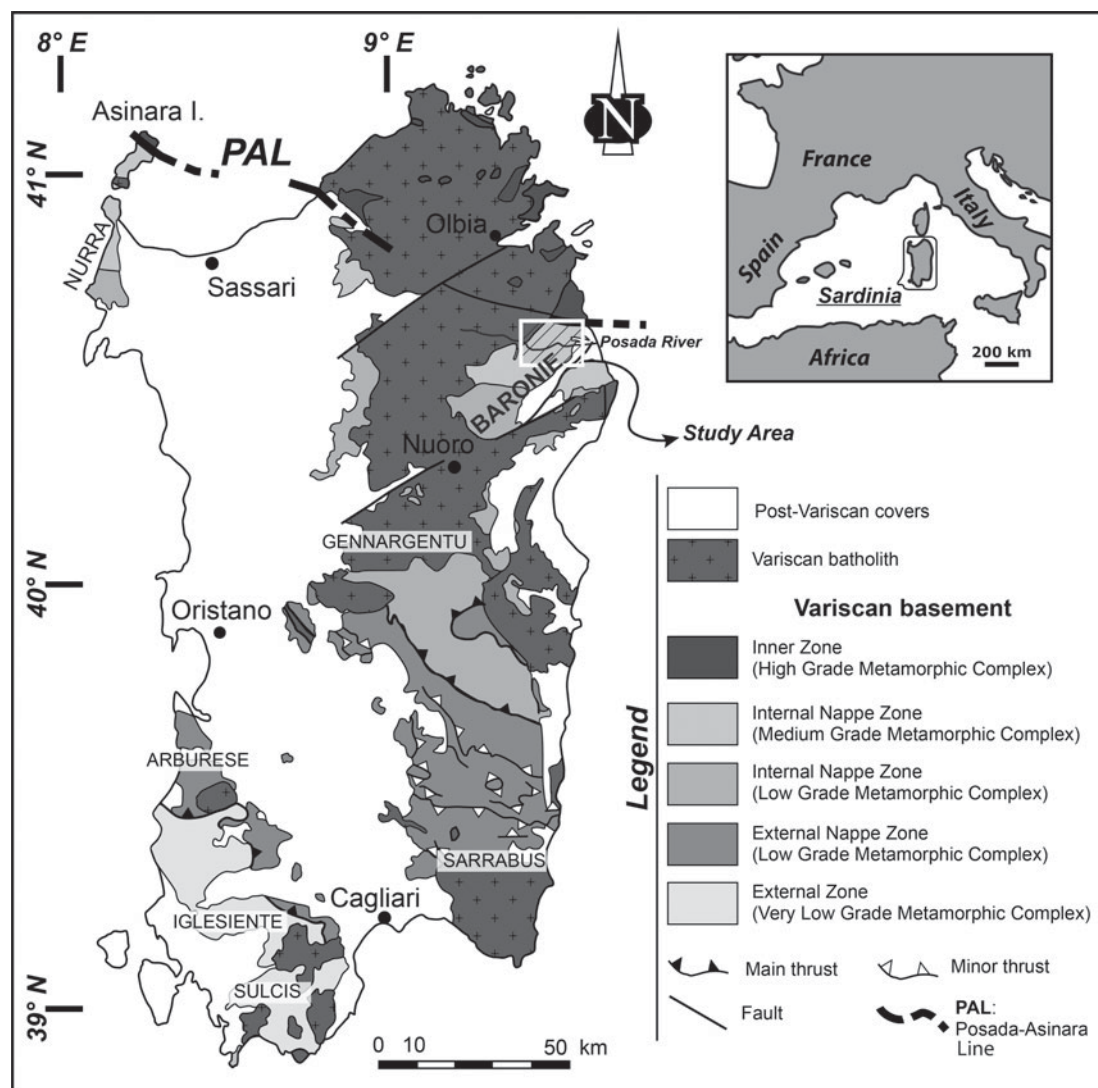


Fig. 1. Sketch-map of the Variscan Belt in Sardinia (modified after Carmignani *et al.* 2001) and location of the study area (white square).

thickening (Matte *et al.* 1998; Carosi & Oggiano, 2002; Carosi & Palmeri, 2002; Carosi *et al.* 2004). Transpressional tectonics also has a profound impact on the metamorphic architecture of an orogenic belt, the latter presenting substantial differences in terms of the tectono-metamorphic evolution compared to perpendicular collisional environments (Thompson *et al.* 1997; Carosi & Palmeri, 2002; Goscombe *et al.* 2003, 2005). Syn-collisional transpression has been investigated in first-order regional-scale shear zones within the main European crystalline basements such as the South-Armorican Shear Zone in Brittany (Gébelin *et al.* 2009); the central sector of the Maures-Tanneron massif in southern France (Corsini & Rolland, 2009; Schneider *et al.* 2014); the Ferrier-Mollières shear zone in the Argentera-Mercantour Massif (Carosi *et al.* 2016; Simonetti *et al.* 2018); and the Posada-Asinara Line (PAL) in northern Sardinia (Carosi & Palmeri, 2002; Carosi & Oggiano, 2002; Carosi *et al.* 2005, 2009; Iacopini *et al.* 2008; Frassi *et al.* 2009; Cruciani *et al.* 2015). In these areas, a major role of transpressive structures related to the exhumation of high- and medium-grade metamorphic complexes has been recognized, well before the onset of the

typical post-collisional extensional events (Turrillot *et al.* 2011; Schneider *et al.* 2014). In this work we investigated an area in NE Sardinia (Fig. 1) where a portion of the PAL, one of the first-order transpressive shear zones of the Variscan Belt in southern Europe, crops out (Corsini & Rolland, 2009; Carosi *et al.* 2015; Simonetti *et al.* 2018). This shear zone has been studied by many authors with respect to the structural settings (e.g. Elter *et al.* 1990), metamorphic evolution, and dynamics and kinematics of flow (e.g. Carosi & Palmeri, 2002; Carosi *et al.* 2005; Iacopini *et al.* 2008; Frassi *et al.* 2009; Cruciani *et al.* 2015). These authors investigated the bulk deformation linked to the transpressive monoclinic flow (Iacopini *et al.* 2008) mainly focusing on the initial conditions of the shearing event at medium T conditions (520–630 °C; Carosi & Palmeri, 2002). The aim of this paper is to fill in the gap concerning the geological history of the long-lasting late transpressive tectonics, constraining the structural evolution and flow kinematics during the latest increments of shear deformation related to the PAL activity.

We present the results of a new structural study on mylonites along the PAL, metamorphosed under medium-grade conditions,

coupled with microstructural analyses including the study of quartz crystallographic preferred orientation (CPO). Quartz petrofabric data allowed us to infer the deformation temperatures and the kinematic vorticity of the flow. Moreover we estimated for the first time the flow stresses and the strain rate along a N–S profile of the PAL, applying published recrystallized grain-size palaeopiezometers for quartz and wet-quartzite flow.

Combining our structural and petrofabric data with the existing published dataset, we propose an updated model of the PAL tectonic evolution and its role in the exhumation/extrusion of metamorphic complexes in orogenic belts.

2. Geological setting

2.a. Overview of the Variscan Belt in Sardinia

The Variscan Belt in Sardinia (Italy) is one of the most complete transects of the Southern Variscan Domain (Matte, 1986; Carmignani *et al.* 1994, 2001; Corsini & Rolland, 2009; Cruciani *et al.* 2015) characterized by a general lack of strong Alpine–Apenninic reworking. The current position of Sardinia derives from a 30° anticlockwise rotation of the Corsica–Sardinia microplate, related to the opening of the Balearic basin (Alvarez, 1972; Montigny *et al.* 1981; Deino *et al.* 2001; Gattacceca, 2001) in the Oligocene Period. Variscan Sardinia consists of metasedimentary and metaigneous rocks of the northern margin of Gondwana, affected by Palaeozoic deformation from the Devonian to Carboniferous periods, related to the collision between Gondwana, Armorica and Laurussia (Carmignani *et al.* 1982, 1994, 2001). During the collision, the Gondwanan margin was the lower plate subducting under Armorica and the peri-Gondwanan terranes, accommodating most of the deformation (Matte, 1986). The Variscan Orogeny is responsible for the main deformation and metamorphic features of Sardinia, consisting of a S- to SW-verging stacking of tectonic units with an increasing metamorphic grade moving from the SW to NE (Carmignani *et al.* 1982, 1994; Franceschelli *et al.* 1982).

The Sardinian basement represents the eastern portion of the inner Ibero-Armorican indenter (Matte, 1986; Carosi & Palmeri, 2002; Cruciani *et al.* 2015), and it can be subdivided into three areas characterized by a different tectono-metamorphic evolution (Carmignani *et al.* 1982, 1994, 2001; Cruciani *et al.* 2015). Along a S to N structural profile, the three areas are (Fig. 1):

(i) The foreland area (External Zone), restricted to SW Sardinia, composed of a poly-deformed Palaeozoic sequence showing very low- to low-grade metamorphism (e.g. Carmignani *et al.* 1994; Franceschelli *et al.* 2017 and references therein).

(ii) A SW-verging nappe stack in the central area constituted by Palaeozoic metasedimentary and metaigneous rocks with low- to medium-grade metamorphism (Carmignani *et al.* 1994; Carosi & Pertusati, 1990; Carosi *et al.* 1991; Montomoli *et al.* 2018). This area is subdivided into two sectors: the External and the Internal Nappe zones. The Internal Nappe Zone has also been subdivided into the ‘Medium-Grade Metamorphic Complex’ and the ‘Low-Grade Metamorphic Complex’ characterized, respectively, by medium- and low-grade metamorphic imprints.

(iii) The Inner Zone, or High-Grade Metamorphic Complex, in the northernmost sector of the island, represented by high-grade metamorphic rocks (Franceschelli *et al.* 1982, 2005; Cruciani *et al.* 2015).

This architecture is intruded by late- to post-Variscan granitoids (Ghezzi *et al.* 1979; Macera *et al.* 1989; Casini *et al.* 2015).

2.b. Northern Sardinia

Northern Sardinia is divided into areas with different metamorphic signatures (Fig. 1): the Internal Nappe Zone represented by the Low- and Medium-Grade Metamorphic complexes (L–MGMC) and the Inner Zone represented by the High-Grade Metamorphic Complex (HGMC) (Cruciani *et al.* 2015 and references therein). The HGMC is located in the northernmost part of the island and consists of migmatites, orthogneisses, amphibolites, minor paragneisses and micaschists, calcsilicates and Carboniferous granitoids (Carmignani *et al.* 1994, 2001; Casini *et al.* 2012). The HGMC experienced an early high-pressure (HP) eclogitic stage (700–740 °C and >1.5 GPa; see Cruciani *et al.* 2015 for a review) followed by a HP granulitic event (660–730 °C, 0.75–0.90 GPa; Miller *et al.* 1976; Ghezzi *et al.* 1979; Franceschelli *et al.* 1982; Di Pisa *et al.* 1993; Cruciani *et al.* 2015) as suggested by granulitized relics of eclogite-facies metabasite embedded within the migmatite. Metamorphic ages are available only for the granulitic event that is constrained at ~350 Ma (Giacomini *et al.* 2005) or younger at ~330 Ma (Palmeri *et al.* 2004). Southwards, the L–MGMC, made up of lower Palaeozoic metasedimentary rocks intruded by Ordovician metagranitic bodies, crops out (Carmignani *et al.* 1994, 2001). The metasedimentary rocks consist of greenschist- to amphibolite-facies micaschists and paragneisses characterized by an increasing Barrovian metamorphic grade from south to north (Franceschelli *et al.* 1982, 1989; Cruciani *et al.* 2015). The metamorphic zoning in the L–MGMC comprises, moving northward, a garnet + albite zone, garnet + oligoclase zone, staurolite + garnet + biotite zone, kyanite zone and sillimanite zone (Franceschelli *et al.* 1982, 1989; Carmignani *et al.* 2001; Cruciani *et al.* 2015). Close to the sheared contact between the two metamorphic complexes, the Barrovian isograds are very tight (Carosi & Palmeri, 2002; Carosi *et al.* 2005). The boundary between the HGMC and L–MGMC is represented by the PAL. The PAL (Fig. 1) is a nearly 150 km long and 10–15 km wide dextral transpressive shear belt crossing the whole of northern Sardinia from Asinara island in the NW to the Posada River Valley in the NE (Cruciani *et al.* 2015). This structure is variably oriented (Fig. 1) from E–W to NW–SE and steeply dips to the south in the NE part (Carosi & Palmeri, 2002). The PAL was originally interpreted as a strike-slip shear zone active in Late Carboniferous time (Elter *et al.* 1990), and later as a wide transpressional shear zone (Carosi & Palmeri, 2002; Iacopini *et al.* 2008; Carosi *et al.* 2009; Frassi *et al.* 2009). Cappelli *et al.* (1992) interpreted the PAL as an oceanic suture zone between Armorica and Gondwana because of the occurrence of amphibolitic boudins aligned along it. The amphibolites show a normal mid-ocean ridge basalt (N-MORB) geochemical signature and locally preserve relics of eclogite facies (Oggiano & Di Pisa, 1992; Cortesogno *et al.* 2004). Recent geochemical constraints attributed the HGMC to the northern margin of Gondwana, confirming the PAL as an intracontinental orogen-parallel shear zone (Giacomini *et al.* 2006). *In situ* Ar–Ar dating of white mica (Di Vincenzo *et al.* 2004) and U–(Th)–Pb dating of monazite (Carosi *et al.* 2012) constrained the age of the transpressional shearing to between ~300 Ma and 320 Ma. These authors recognized the presence of two main deformation phases associated with the Variscan tectonic evolution: a regional D1 phase associated with the collisional stage recognizable all across the whole of Sardinia, and a later orogen-parallel D2 phase linked to the transpressive activity. Based on pseudosection calculations, a prograde HP metamorphic signature (1.8 GPa and 460–500 °C) has been recognized by Cruciani *et al.* (2013) for the D1, allowing the linking of

this phase to prograde metamorphism related to underthrusting and nappe stacking. The age of the D1 is ~330–340 Ma (Di Vincenzo *et al.* 2004; Carosi *et al.* 2012). The transition between D1 and D2 represents a change in metamorphic conditions from high pressure to lower pressure with increasing temperature during decompression (Carosi & Palmeri, 2002; Cruciani *et al.* 2013, 2015) followed by decompression and cooling.

2.c. Study area (Baronie Region)

The study area is located within the northern sector of the L–MGMC and comprises part of the garnet + plagioclase zone and the garnet + staurolite + biotite zone, a few kilometres south of the boundary with the HGMC (Fig. 2) where a detailed geological and structural map (at the scale of 1:5000) was compiled.

The structural setting is dominated by N–NE-verging regional-scale isoclinal folds with axial planes striking N20–90° and dipping 20–80° to the SE (Fig. 2b). In the core of the antiforms an orthogneiss body crops out with a protolith age of 456 ± 14 Ma (Helbing & Tiepolo, 2005). It is composed of granodioritic orthogneiss (Fig. 3a) at the base, surrounded by granitic augen orthogneiss (Fig. 3b). The northern area and the cores of the synforms expose Pre-Cambrian (?) to Cambrian micaschist (Fig. 3c, d) with paragneiss and quartzitic lenses (Carmignani *et al.* 1994). In the southern area the micaschist is affected by a low- (garnet + albite) to medium- (garnet + oligoclase) grade metamorphism. The medium-grade metamorphic conditions in the micaschist, cropping out in the northern area, are evident from the garnet + staurolite + biotite metamorphic assemblage.

3. Deformation history and structural analysis

On the basis of geological mapping, as well as of detailed meso- and microstructural analyses, five ductile deformation phases, followed by brittle tectonics, have been identified. All microstructural observations have been conducted on thin-sections cut perpendicular to the main foliation and parallel to the mineral lineation to better approximate the XZ section of the finite strain ellipsoid.

The first deformation phase is recognizable mainly at the microscale and it is poorly expressed at the mesoscale. It is represented by a relict foliation, S1, within D2 microlithon domains and by internal foliations, S_i , within garnet, staurolite and plagioclase intertectonic porphyroblasts. This phase is related to the syn-kinematic growth of white mica, biotite, feldspar and garnet in the micaschist.

In the study area the prominent deformation event is the second deformation phase (D2), associated with the development of isoclinal folds (F2). The F2 folds have similar geometry (Ramsay, 1967); they are non-cylindrical, trending N080–090° with axes showing variable plunge, from horizontal in the western area to 30–40° to the east in the eastern area (Fig. 2a). The F2 axial planes (Ap2) strike mostly N080–090°. In the eastern sector they strike N010–020°. The Ap2 dips 70–80° to the south in the northern sector of the area, and 10–20° to the south in the southern sector (Fig. 2b). This variation is owing to the presence of late deformation events (D4 and D5) deforming their original attitude (see below). The main foliation of the study area, S2, shows a mylonitic fabric. Within the orthogneiss, the S2 foliation is a discrete spaced schistosity, marked by the alternation of mica-rich cleavage domains and quartz-feldspathic microlithons. Within the micaschist, S2 varies from a continuous to a spaced foliation. In domains of spaced foliation, the S2 is characterized by

anastomosing biotite- and white mica-bearing lepidoblastic layers alternated with lenticular microlithon domains (Fig. 4a, b), where S1 relics are present.

The D2 mylonitic fabric is well recognizable at all scales. Shear sense indicators have been observed only on sections parallel to the XZ plane of the finite strain ellipsoid (i.e. perpendicular to the S2 foliation and parallel to mineral lineation) and they have not been detected on YZ and XY sections.

S-C-C' structures, mica fishes (mainly of groups 1, 2 and 3 according to the classification of ten Grotenhuis *et al.* 2003), asymmetric strain shadows around porphyroblasts and oblique foliations point to a dextral sense of shear consistent with the top-to-the-W/NW direction of tectonic transport associated with the PAL (Fig. 4a–e). Elongation of feldspar, garnet and staurolite crystals on the S2 planes form a sub-horizontal L2 mineral/grain and aggregate lineation (average plunge 0–10° to the E).

The M2 metamorphism is related to the syn-kinematic growth of the main mineral assemblages (biotite + white mica + garnet + plagioclase + quartz in the southern sector and biotite + white mica + garnet + staurolite + quartz in the northern sector). A late syn-kinematic growth of chlorite on the late shearing planes (mainly C' planes and shear bands), in the strain shadows around garnet (Fig. 4d, e) and filling fractures in garnet and staurolite has been recognized. This retrogression is present in the studied transect and highlights a progressive decrease in metamorphic grade during D2, starting from lower amphibolite to greenschist facies. Interlobate to ameboidal grain boundaries in quartz ribbons are consistent with grain boundary migration (GBM) recrystallization (Stipp *et al.* 2002a,b; Law, 2014).

The presence of finer equigranular quartz grains along the grain boundaries suggests superposition of subgrain rotation (SGR) recrystallization, which heterogeneously reworks and overprints the GBM microstructures in all the studied samples (Fig. 5a–c). Although SGR occurs in all of the study area, in the N–S transect the intensity of SGR varies from incipient in the southern sector (Fig. 5a) to pervasive in the northern sector, where core and mantle structures (Fig. 5b) or nearly complete recrystallization (Fig. 5c) are present.

The D3 phase is characterized by a heterogeneous deformation localized in E–W-trending lenticular domains developed at the hectometric scale. Here an S3 crenulation cleavage (Fig. 3e, f), linked to centimetric- to hectometric-scale F3 similar folds (Ramsay, 1967) occurs (Fig. 4f). F3 axial planes (Ap3) and S3 foliation are parallel to S2 mylonitic foliation. F3 folds have a non-cylindrical geometry, and the plunge of the A3 axes varies from sub-vertical to a few degrees to the east. The parallelism between the S2 and S3 foliation planes, and the scattering of the A3 axes along the S2 great circle (Fig. 2a) on the stereographic projection, point to a similar geometry and kinematics of deformation during the D2 and D3 phases. At the microscale, the S3 is a crenulation cleavage characterized by pressure solution and by a shape preferred orientation (SPO) of quartz aggregates (Fig. 5d). Pressure solution and quartz deformation mechanisms acting during the D3 phase suggest shallower conditions with respect to the D2 phase.

The D4 deformation event is detectable only at the map scale by the occurrence of gentle kilometric folds. The F4 folds cause the variation of S2 strike from N080–090° up to N000–010° (Fig. 2a). The F4 axial planes (Ap4) strike about N135°/55° NE while the A4 axes trend N105°, plunging 35° to the SE. No axial plane foliation is observed parallel to the F4 axial planes.

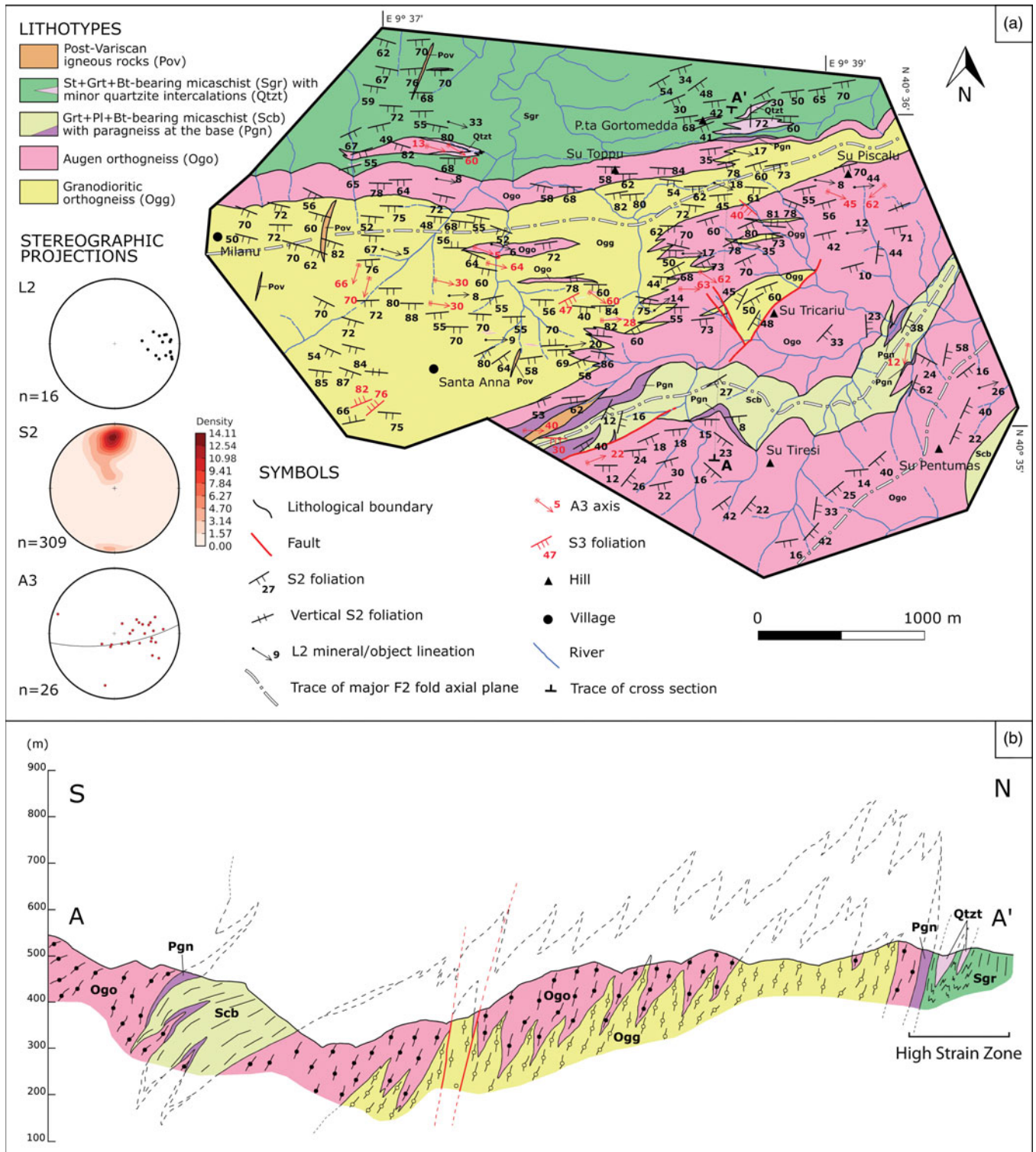


Fig. 2. (Colour online) (a) Geological map of the study area. The central granodioritic orthogneiss antiform separates micaschist with different metamorphic assemblages: garnet + plagioclase + biotite in the southern portion and garnet + staurolite + biotite in the northern area. Lower hemisphere stereographic projections for L2: mineral and object lineations related to D2; A3: fold axes related to F3 folds; S2: poles to the main foliation, S2. (b) N-S geological cross-section of the studied area (see trace A-A' in Fig. 2a). The main deformation style is characterized by N-verging F2 isoclinal folds with steeply S-dipping axial planes in the southern area, and a more gentle S-dipping axial planes in the northern area, and a crenulation belt, related to the D3, is highlighted.

The D5 deformation phase is characterized by meso- to map-scale folds. The F5 folds have a gentle to close geometry with a sub-horizontal axial plane and N88°-trending axes slightly plunging to the east. The variation in the dip of the S2 mylonitic foliation

is due to later F5 folds producing type 3 interference structures when overprinting the F2 folds (Fig. 2b). Foliations and lineations related to the D5 phase have not been detected in the study area. This observation, coupled with the absence of mineral growth or

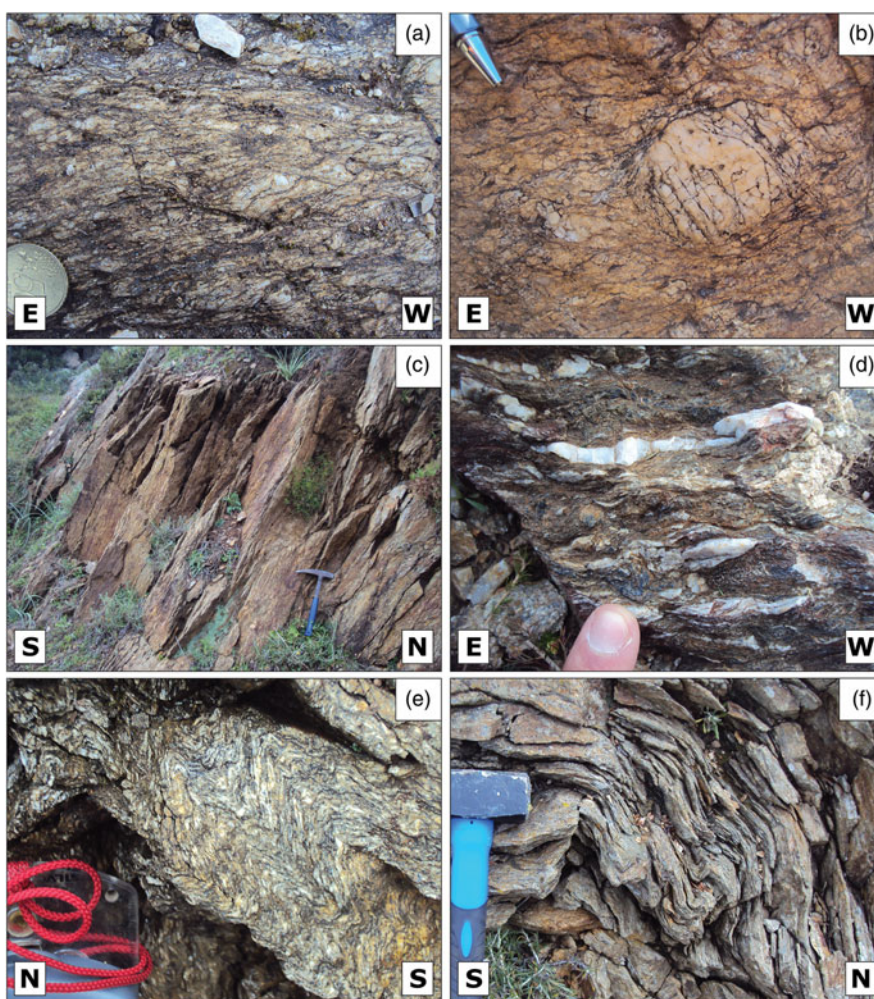


Fig. 3. (Colour online) Main lithotypes in the study area. (a) Biotite-rich granodioritic orthogneiss (coin for scale is 2.3 cm diameter). (b) Augen orthogneiss with K-feldspar porphyroclasts (pencil tip for scale is 3 cm long). (c) Garnet + plagioclase-bearing micaschist (hammer for scale is 32 cm long). (d) Garnet + staurolite + biotite-bearing micaschist (fingernail for scale is ~1.2 cm wide). In some specific areas, S3 crenulation cleavage is affecting, respectively, (e) orthogneiss (compass for scale: visible upper side is ~3.2 cm long) and (f) micaschist (hammer for scale is 30 cm long).

related microstructures, suggests that D5 took place at shallow structural levels. The D5 phase has been associated with the late exhumation related to the final collapse of the Sardinian Variscan Belt (Carmignani *et al.* 1994).

Evidence of brittle deformation is poorly represented in the study area. In the southeastern portion of the study area (Fig. 2a), conjugated normal faults have been detected. They strike N045° and N155° and steeply dip, respectively, to the NW and NE (Fig. 2a).

4. EBSD analysis and quartz petrofabric

4.a. Methods

Of the 39 rock specimens (Fig. 6) used for the microstructural analysis, ten representative samples of the main lithotypes were selected to investigate the rheological behaviour of quartz during the deformation. On these samples we performed image analyses using the software ImageJ (ver: 1.47v by Wayne Rasband).

For each specimen, several statistics images away from quartz ribbon areas (Fig. 7) were processed to estimate the amount of quartz in the matrix. All the analysed samples show a modal abundance of quartz in the matrix ranging between 24 % and 81 % (Fig. 8; Table 1). Following a microstructural analysis on the complete dataset and the modal estimates, three quartz-rich samples were selected for the CPO study.

These samples contain polycrystalline quartz ribbons recrystallized during the D2 phase (Fig. 8). The analysed samples were selected at different distances from the high-strain zone (Fig. 7) within the three main lithotypes occurring in the study area: SCB006R from the garnet + plagioclase zone (southern area); OGO026R from the augen orthogneiss zone (central area); and SGR031R from the garnet + staurolite + biotite zone (northern area) (Fig. 6). The electron backscatter diffraction (EBSD) analysis was performed on selected areas representative of the SGR recrystallization domains, related to the late D2 phase, in order to better constrain the late-D2 deformation event (Fig. 8).

EBSD analysis was performed on carbon-coated polished thin-sections using a JEOL 6610 scanning electron microscope (SEM) at the Plymouth University Electron Microscopy Centre, with the following working conditions: acceleration voltage of 20 kV, high vacuum and 70° sample tilt. EBSD patterns were acquired on rectangular grids ~6–9 mm² in size (Fig. 8), with an electron beam step-size of 3.5–5.0 μm.

The bulk CPO data have been represented with pole figures of the main crystallographic elements of quartz: c axis <0001>, a axes {11–20} and m planes {10–10}. The orientation data have been plotted as one point per grain. The EBSD results have also been shown as inverse pole figure (IPF) crystallographic maps to visualize the spatial distribution of the CPO domains (Fig. 9).

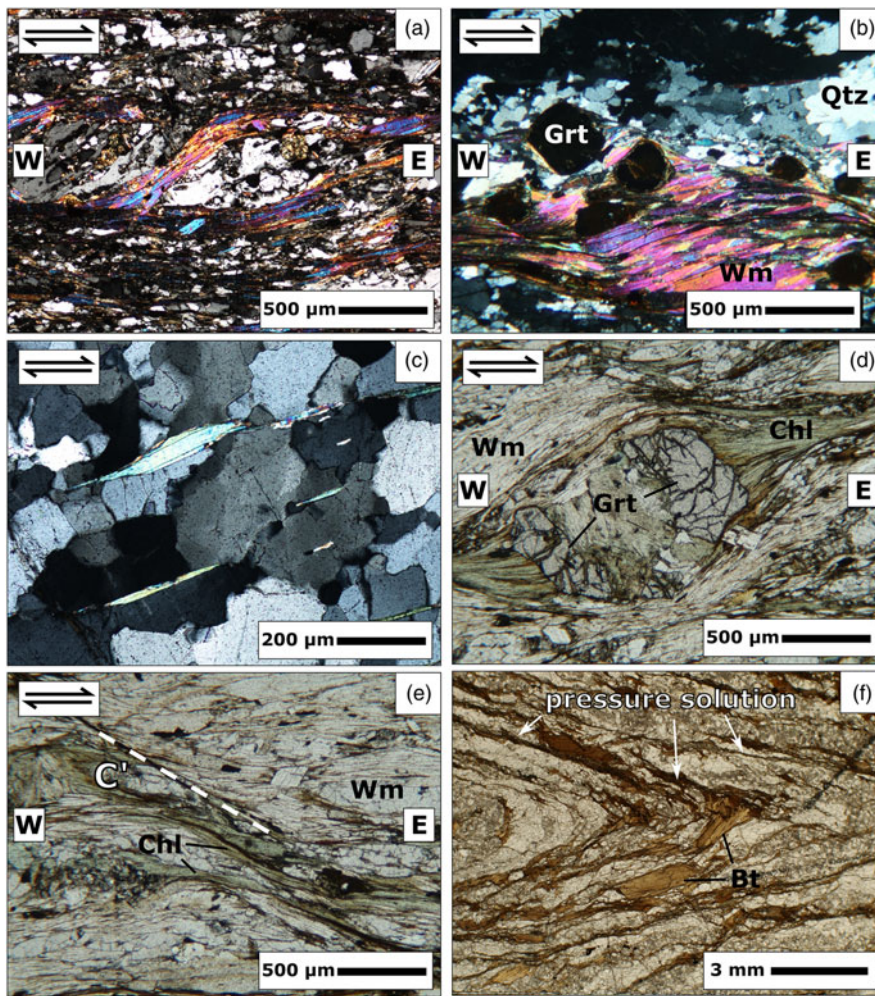


Fig. 4. (Colour online) Microstructures associated with the main deformation events present in the study area from the (a–c) early D2 stage to the (d–e) late D2 stage and (f) D3 phase. (a) S–C fabric in garnet + plagioclase-bearing micaschist with S planes composed of biotite and white mica. Dextral sense of shear, corresponding to a top-to-the-W and -NW sense of shear in the field (mylonitic foliation steeply dips to the south) (crossed nicols). (b) Biotite and white mica foliation fish in garnet + staurolite + biotite-bearing micaschist (crossed nicols). (c) Mica fishes (group 1 and 2) in a quartz-rich matrix (ten Grotenhuis *et al.* 2003) (crossed nicols). (d) Garnet porphyroclast in garnet + plagioclase-bearing micaschist with syn-D₂late growth of chlorite in fractures and strain shadows (parallel nicols). (e) C' plane with syn-kinematic growth of chlorite in garnet + plagioclase + biotite-bearing micaschist (parallel nicols). (f) F3 centimetre fold in the granodioritic orthogneiss. Furthermore, it is also possible to note how the D3 event is associated with pressure solution as the main deformation mechanisms (parallel nicols). Mineral abbreviations: Grt – garnet; Qtz – quartz; Wm – white mica; Chl – chlorite; Bt – biotite.

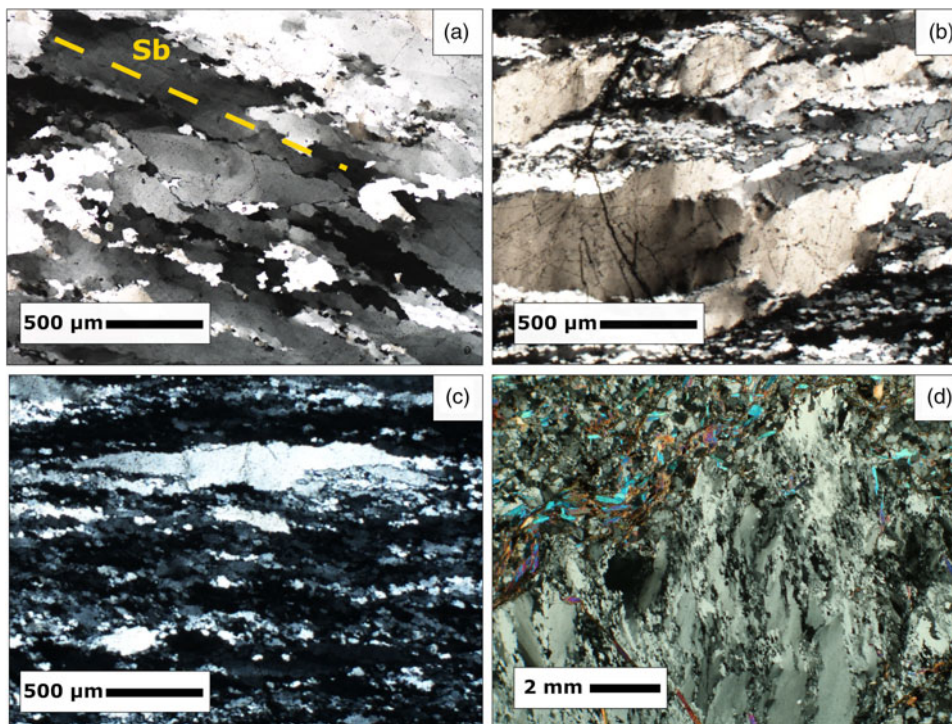


Fig. 5. (Colour online) General overview of syn-D2 quartz microstructures recognized in the study area along samples collected at different distances from the high strain zone of the PAL (i.e. boundary between L-MGMC and HGMC). (a) Southern sector of the study area: quartz microstructures are dominated by GBM recrystallization with incipient SGR. Sb represents the oblique foliation due to the shape preferred orientation (SPO) of quartz aggregates (crossed nicols). (b) Central sector of the study area: SGR microstructures are more developed (crossed nicols). (c) In the northern sector of the study area, close to the high strain zone, the SGR process is pervasive and completely obliterates GBM microstructures (crossed nicols). (d) Plastic deformation in quartz within the hinge zone of an F3 fold where the SPO of quartz crystals is parallel to the S3 foliation (crossed nicols).

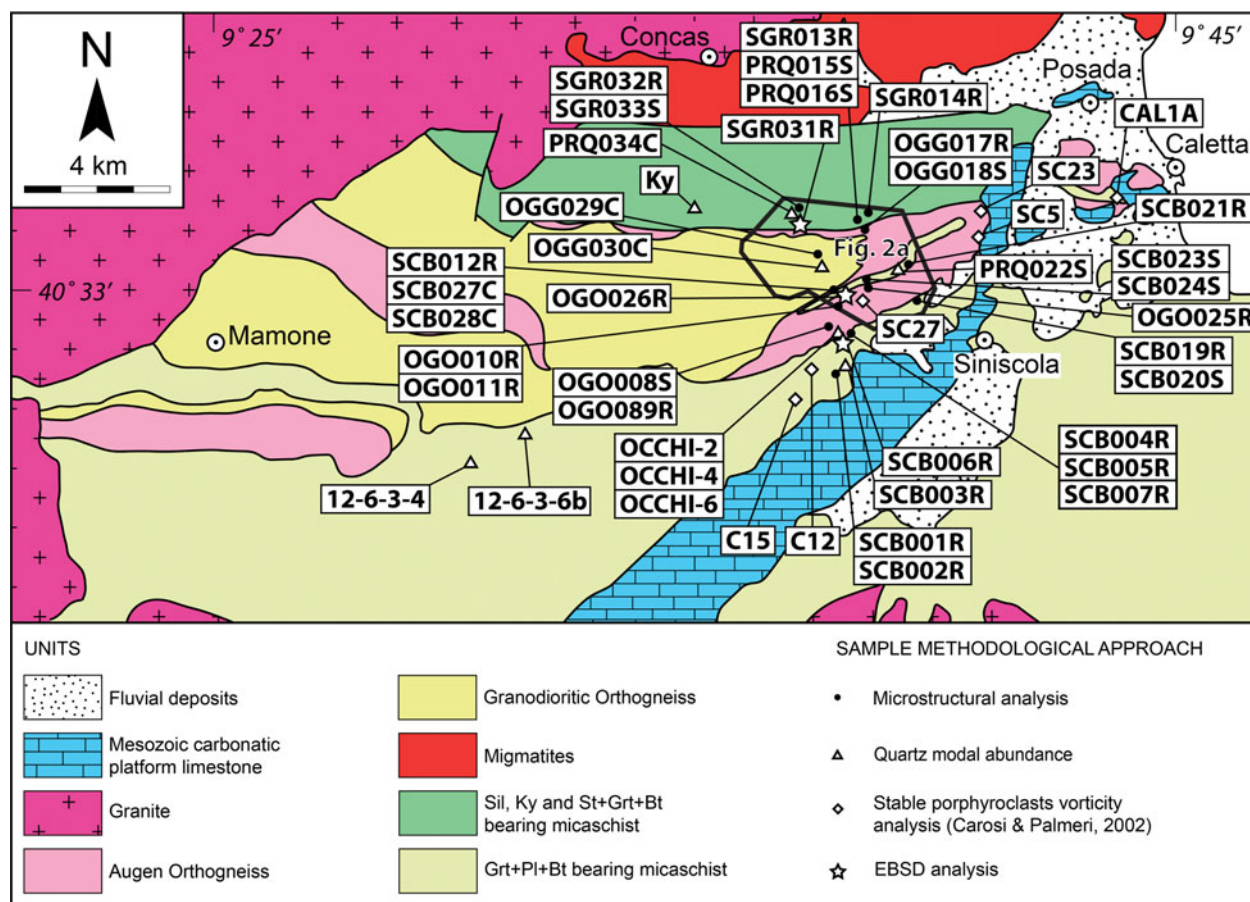


Fig. 6. (Colour online) Geological sketch map of the Baronie region showing sample dataset and location of the samples selected for specific analyses (modified from Carosi *et al.* 2005). Abbreviations: Sil – sillimanite; Ky – kyanite; St – staurolite; Grt – garnet; Pl – plagioclase; Bt – biotite.

4.b. Crystallographic preferred orientation data

The distribution of the quartz *c* axes is similar for the three analysed samples. Both SCB006R and SGR031R have a type-1 crossed girdle transitional to single girdle distribution (Fig. 9a, c) (Lister & Hobbs, 1980; Schmid & Casey, 1986; Passchier & Trouw, 2005, p. 104; Toy *et al.* 2008). OGO026R presents an incomplete *c*-axes distribution owing the larger grain size compared to the other samples. Type-1 crossed girdle distributions suggest a plane strain deformation (Lister & Hobbs, 1980; Schmid & Casey, 1986). The asymmetry of the distribution points to a non-coaxial regime (Law, 1990; Passchier & Trouw, 2005, p. 105) with a top-to-the-W sense of shear, in agreement with independent kinematic indicators (see above) and consistent with the D2 phase. Despite the incomplete data, a type-1 crossed girdle distribution is still recognizable.

The pole figures and the IPF maps are consistent with the dominant activity of the rhomb<a> slip system, with a lesser contribution of prism<a> and basal<a> (Fig. 9a, b) (Toy *et al.* 2008; Fazio *et al.* 2017; Hunter *et al.* 2018). These data, under typical geological conditions for H₂O content and geological strain rate, suggest a deformation temperature in the upper greenschist facies (e.g. Passchier & Trouw, 2005, p. 57; Toy *et al.* 2008). Deformation temperatures (*T_d*) have been estimated using the relationship between *T_d* and the opening angle (OA) of the *c*-axes distribution (Fig. 9c) (Kruhl, 1998; Morgan & Law, 2004; Law, 2014) with the most recent, pressure sensitive, calibration proposed by Faleiros *et al.* (2016):

$$T_d = 410.44 \ln(OA) + 14.22P - 1272$$

To estimate the *T_d* with this relationship, an external pressure constraint (*P*) is necessary. In this work, the *P* constraint has been obtained from the data of Carosi & Palmeri (2002), who estimated a pressure of 0.7 GPa for the D2 peak. Moreover, considering that the late recrystallized areas developed under retrograde greenschist facies, the rocks deformed during the late D2 phase were likely under lower pressure conditions compared to the peak conditions. For this reason, a more realistic *P* of 0.5 GPa has been also assumed (based on *P*–*T* paths of Carosi & Palmeri, 2002) for the calculations. The estimated temperatures at the corresponding *P* of 0.5 GPa for SCB006R and SGR031R are 400 ± 50 °C and 390 ± 50 °C, respectively. The estimations for OGO026R were not possible owing to the incomplete nature of the *c*-axes distribution. These temperatures estimated using 0.5 GPa as the pressure constraint do not present a significant deviation (less than 30 °C) from those obtained at the corresponding pressure of 0.7 GPa. These data do not show large variations from the *T_d* values obtained by the original Kruhl (1998), as modified by Morgan & Law (2004), calibration. The results obtained by the different calibrations and pressure values are well within the error range of the method (± 50°; see also Law, 2014). The *T_d* data are consistent with the estimated greenschist-facies conditions, and indicate a homogeneous deformation temperature in the study area along the N–S transect, as also supported by the late syn-D2 greenschist minerals.

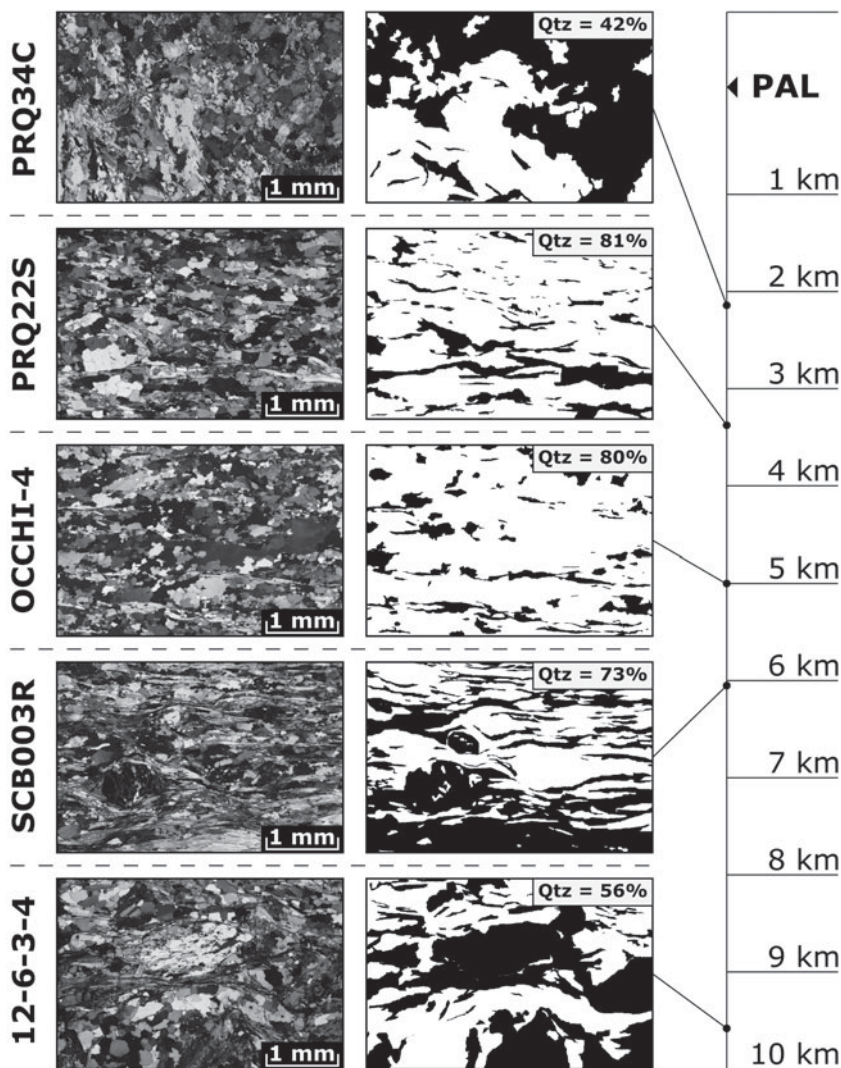


Fig. 7. Examples of quartz (Qtz) modal analysis on rock specimens homogeneously distributed along the studied transect. In all the analysed samples, quartz (white in processed figures) represents an important volumetric phase in the rocks and it is typically distributed in interconnected granoblastic layers (see Table 1 for the complete dataset and Fig. 6 for sample locations).

4.c. Kinematic vorticity data

The kinematic vorticity represents the magnitude of the kinematic vector, which the material lines tend to rotate around during flow deformation (Xypolias, 2010 and references therein). The kinematic vorticity number (indicated as W_n , for single deformation increments) is identified by the cosine of the angle between the two flow apophyses. Kinematic vorticity is an estimate of the relative contribution of pure and simple shear components during the flow.

Quartz CPO data have been used to estimate the components of simple and pure shear of the flow kinematic during the late D2 deformation increments (Wallis, 1995; Law *et al.* 2004, 2010, 2011, 2013; Xypolias, 2010). This estimate has been performed by calculating the sectional kinematic vorticity number (W_n) on recrystallized quartz domains using the β/δ method (Fig. 10) proposed by Xypolias (2010) (see also Wallis, 1995), where:

$$W_n = \sin[2(\delta + \beta)]$$

In this equation, β is the angle between the main foliation and the plane normal to the quartz *c*-axes distribution (Figs 9c, 10b), while δ is the highest angle between the main foliation and the SPO

foliation of quartz aggregates (Fig. 10a, b). δ has been derived from a range of angles measured via optical microscopy (Fig. 5a).

This method is based on the relationship between the simple shear component and the angle between the flow apophysis, A_2 , highlighted by the orientation of the quartz CPO and the instantaneous stretching axis, ISA_2 , represented by the oblique foliation. Showing the main flow elements in the Mohr space (Fig. 9c), the W_n can be obtained by the sine of the angle between A_2 and ISA_2 . The kinematic vorticity estimations (Fig. 11) provided $W_n = 0.99-1.00$ for SCB006R, $W_n = 0.91-1.00$ for OGO026R and $W_n = 0.99-1.00$ for SGR031R. The obtained W_n values point to very high components of simple shear for all samples.

4.d. Palaeopiezometry and strain rate

Following the pioneering analysis of Twiss (1977) it has been suggested that the grain size of recrystallized grains is a primary function of the applied flow stress, representing the theoretical base of palaeopiezometry (Behr & Platt, 2011, 2013, 2014; Menegon *et al.* 2011; Boutonnet *et al.* 2013). The grain-size distribution of the analysed quartz aggregates (Fig. 12a) was derived for each sample with the aid of the EBSD data. These distributions have been used to estimate the flow stress acting during the recrystallization process

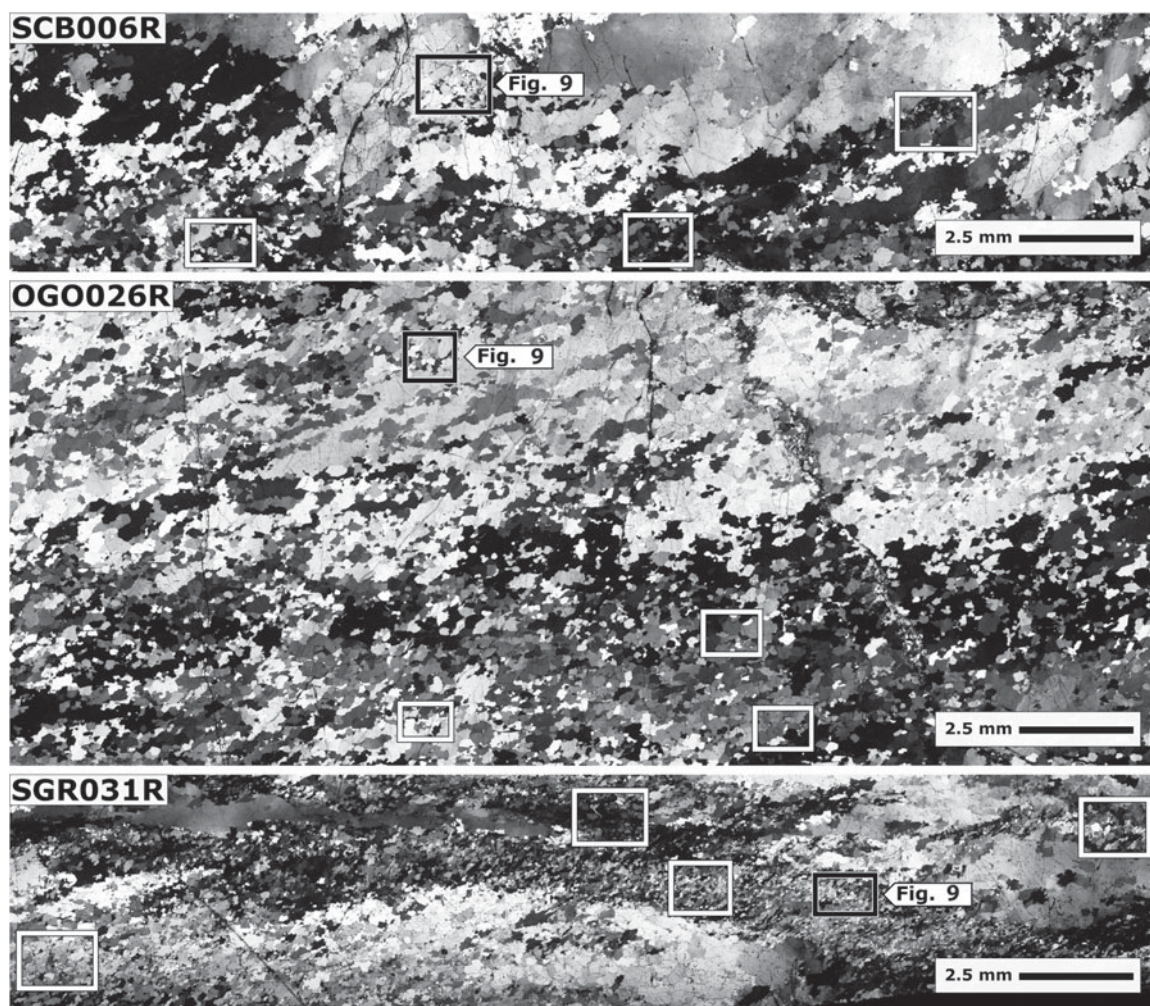


Fig. 8. Localization of the acquired EBSD maps on the analysed samples (crossed nicols). Black boxes indicate the representative maps chosen for Figure 9. White boxes indicate the other areas where EBSD data have been acquired to reach a statistical number of points to build the pole figures in Figure 9.

related to the late D2 activity of the PAL. For this purpose, we used the recrystallized grain-size palaeopiezometer for quartz proposed by Stipp & Tullis (2003) for the recrystallization regime 2/3, where:

$$D = 3631\Delta\sigma^{-1.26}$$

With this relationship, the flow stress ($\Delta\sigma$) can be obtained from the average recrystallized grain diameter (D). The calculated values were: $D = 34 \pm 16 \mu\text{m}$ and $\sigma = 41 \pm 18 \text{ MPa}$ for SCB006R; $D = 25 \pm 6 \mu\text{m}$ and $\sigma = 53 \pm 11 \text{ MPa}$ for OGO026R; and $D = 16 \pm 4 \mu\text{m}$ and $\sigma = 74 \pm 16 \text{ MPa}$ for SGR031R, showing an increase in flow stress moving from the southern to the northern sectors of the study area, along a N–S transect of the PAL. The flow stress data have been used to calculate the strain rate ($\dot{\epsilon}$) with the wet-quartzite flow law:

$$\dot{\epsilon} = A\Delta\sigma^n (f\text{H}_2\text{O})^m e^{-Q/RT}$$

For the strain rate estimation, a temperature constraint (T) is necessary. The T values used in this work have been obtained from the opening angle of the c -axes distribution (Law, 2014) as described above. A water fugacity ($f\text{H}_2\text{O}$) of 12.25 MPa was calculated using the water fugacity coefficient listed in Tödheide (1972) for

$T = 400 \text{ }^\circ\text{C}$ and $P = 0.5 \text{ GPa}$. Different experimental calibrations for the wet-quartzite flow law have been proposed in the literature (see Table 2, where: A , n and m are experimentally calculated parameters that change for each calibration and R is the ideal gas constant), and they led to dissimilar strain rate estimations (Menegon *et al.* 2011; Boutonnet *et al.* 2013; Montomoli *et al.* 2018).

The results of the different calibrations used in this paper are summarized in Figure 12b. Strain rate estimations cover a wide range, spanning from 10^{-16} to 10^{-11} s^{-1} (including the uncertainties due to the propagation of the error on temperature and flow stress). Although the strain rates estimated using different flow laws are different, they coherently indicate an increasing trend of $\dot{\epsilon}$ moving from south to north (Fig. 12b). Among the different calibrations for the quartzite flow law, the one proposed by Hirth *et al.* (2001) has been selected since, according to Behr & Platt (2013, 2014), it is considered the most realistic (see also Boutonnet *et al.* 2013 for a discussion on this topic). The estimated strain rate values are in the range of 10^{-13} to 10^{-12} s^{-1} (Fig. 12b).

Comparable strain rate results have been reported for the mid crustal shear zone from different areas such as the Betic Cordillera of southern Spain (Behr & Platt, 2013), the Rodope Massif in Greece (Fazio *et al.* 2018), the Kabilo–Calabride crystalline basement in southern Italy (Ortolano *et al.* 2020) and the

Table 1. Modal abundance of quartz along the study transect (see Fig. 6 for sample locations)

Sample	Structural distance (km)*	Lithotype	Unit	%Qtz
Ky	1.59	micaschist	kyanite-bearing micaschist	24.7
PRQ034C	2.15	paragneiss	garnet + staurolite + biotite-bearing micaschist	42.5
OGG030	3.05	orthogneiss	granodioritic orthogneiss	39.4
PRQ022	3.65	paragneiss	garnet + plagioclase-bearing micaschist	81.1
OCCHI-2	4.96	orthogneiss	augen orthogneiss	75.2
OCCHI-4	4.99	orthogneiss	augen orthogneiss	79.7
OCCHI-6	5.01	orthogneiss	augen orthogneiss	58.3
SCB003	5.93	micaschist	garnet + plagioclase + biotite-bearing micaschist	72.9
12-6-3-6b	8.65	micaschist	garnet + plagioclase + biotite-bearing micaschist	34.6
12-6-3-4	9.63	micaschist	garnet + plagioclase + biotite-bearing micaschist	56.0

* The structural distance refers to the relative position with respect to the boundary between the HGMC and L-MGMC.

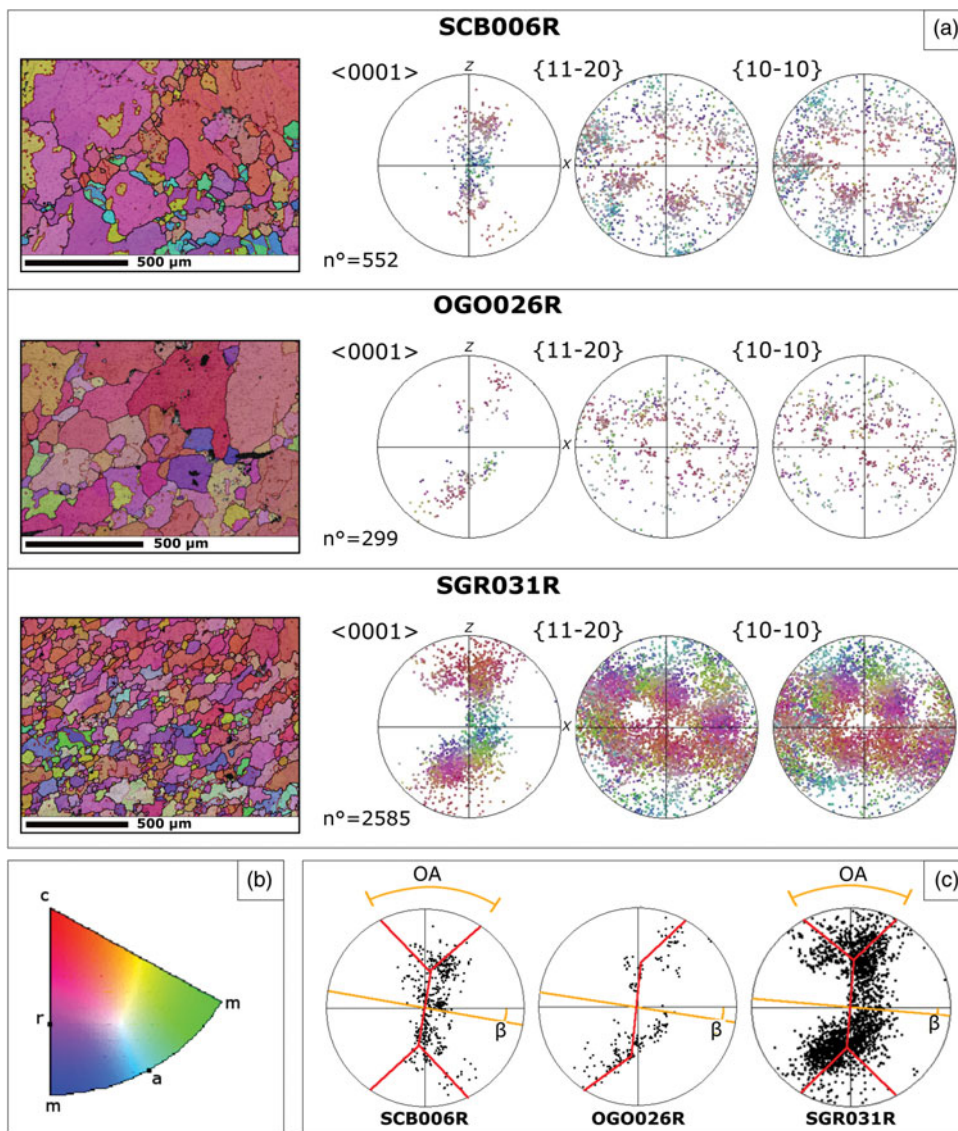


Fig. 9. (Colour online) (a) Quartz EBSD data from the analysed samples (for sample locations see Fig. 8). The colours of the example IPF figures on the left and the pole figures are in reference to the Z axis of the finite strain (pole of the main foliation). Black lines are high-angle boundaries (misorientation $>10^\circ$), fuchsia lines are low-angle boundaries (misorientation $3-10^\circ$) and red lines are Dauphiné twin boundaries (misorientation of 60° around the c axis). The orientation in the pole figures data has been plotted as one point per grain. (b) Legend for the quartz IPF map, showing the main quartz crystallographic directions with different colours. (c) Interpreted quartz c-axes $\langle 0001 \rangle$ patterns of the studied samples. OA – opening angle; β – angle between the mylonitic foliation and the orthogonal plane of the quartz c-axes central girdle.

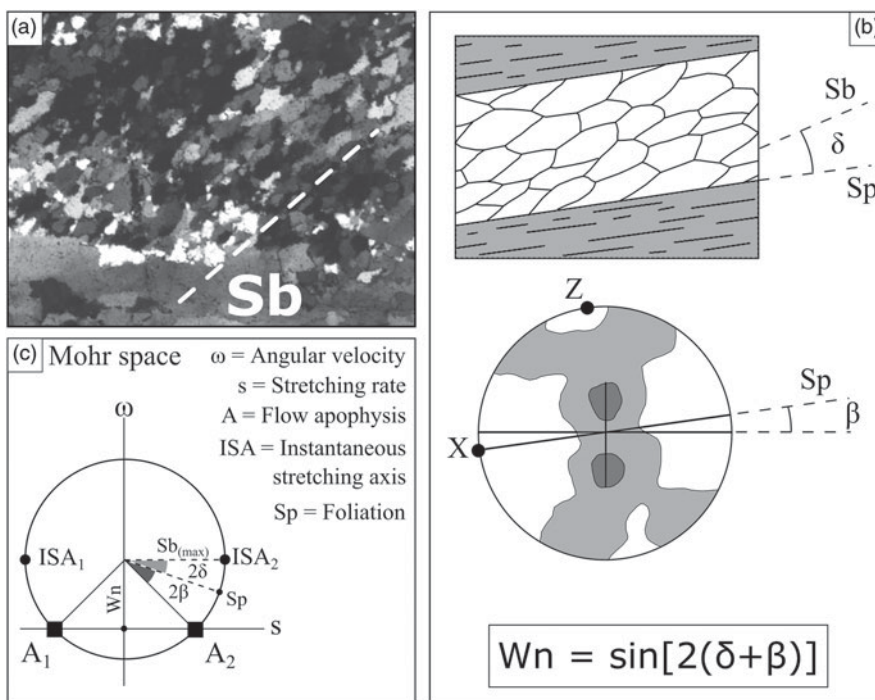


Fig. 10. Schematic representation of the β/δ method (Xypolias, 2009, 2010), applied in the current study, in order to estimate the sectional kinematic vorticity number (W_n) by studying the CPO and SPO of a deformed quartz ribbon. (a) δ is the angle between the mylonitic foliation and the maximum oblique foliation (S_b) in quartz aggregates (microphotograph, crossed nicols, sample SGR031R), (b) while β is the angle between the mylonitic foliation and the orthogonal plane of the quartz c-axes central girdle. (c) Representation of instantaneous and finite elements of flow in Mohr space, with the stretching rate (s) as the horizontal axis and the angular velocity (ω) as the vertical axis; δ represents the angle between the foliation and the instantaneous stretching axis ISA_2 while β represents the angle between the foliation and the flow apophysis A_2 (modified from Xypolias, 2010).

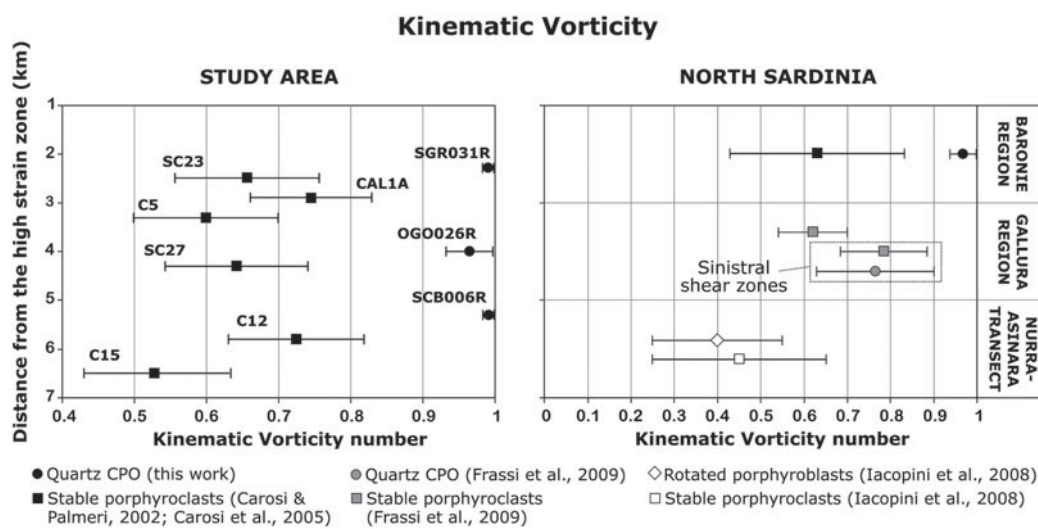


Fig. 11. Comparison between kinematic vorticity data obtained in this work and previous estimates in the same area (left, see Fig. 6 for sample locations) and along the whole PAL profile. Kinematic vorticity data, resulting from the quartz CPO analysis in this work, is higher than the previous data obtained by previous authors both using the quartz-based petrofabric (Frassi *et al.* 2009) and other vorticity gauges (Carosi & Palmeri, 2002; Carosi *et al.* 2005; Iacopini *et al.* 2008).

Chelmos Shear Zone in the External Hellenides (Xypolias & Koukouvelas, 2001).

5. Discussion

5.a. Structural evolution

Our field, meso- and microstructural data document a complex polyphase tectono-metamorphic evolution of the Sardinian Variscan Belt after the collisional stage. The PAL activity is confirmed to be related to the D2 phase, during which micaschist and orthogneiss are deformed under amphibolite-facies conditions, coeval with a non-coaxial dextral transpressive shearing (Carosi & Palmeri, 2002). The syn-kinematic growth of chlorite, in strain shadows and along the C' planes (Fig. 4e), is consistent

with a metamorphic retrogression towards greenschist facies during the evolution of the late D2 phase. The syn-kinematic growth of chlorite during the D2 phase, at the expense of biotite and garnet, supports the presence of H_2O -rich fluids during this phase.

The D3 phase developed heterogeneously in the study area. The parallelism of the structural elements between the D2 and D3 deformation phases allows the D3 to be interpreted as an evolution of the D2 phase linked to the latest deformation increments of the PAL. The D2–D3 transition could be related to a strain hardening due to shallower metamorphic conditions with strain localization and deformation concentrated in parallel crenulated domains (Fig. 13).

The absence of metamorphic assemblages related to the D4 and D5 phases points to a further T decrease associated with the deformation of the L–MGMC at shallower structural levels.

Table 2. Available calibrations for the wet-quartzite flow law and associated experimentally derived flow law parameters*

Flow law calibration	Q (KJ/mol)	A (MPa ⁻ⁿ /s)	m	n
Paterson & Luan (1990)	135	6.50E-08	0	3
Luan & Paterson (1992)	152	4.00E-10	0	4
Gleason & Tullis (1995)	223	0.00011	0	4
Hirth <i>et al.</i> (2001)	135	6.31E-12	1	4
Gleason & Tullis (1995) (corrected by Holyoke & Kronenberg, 2010)	223	0.00051	0	4

* Q – activation energy; A – material parameter; m – water fugacity exponent; n – stress exponent.

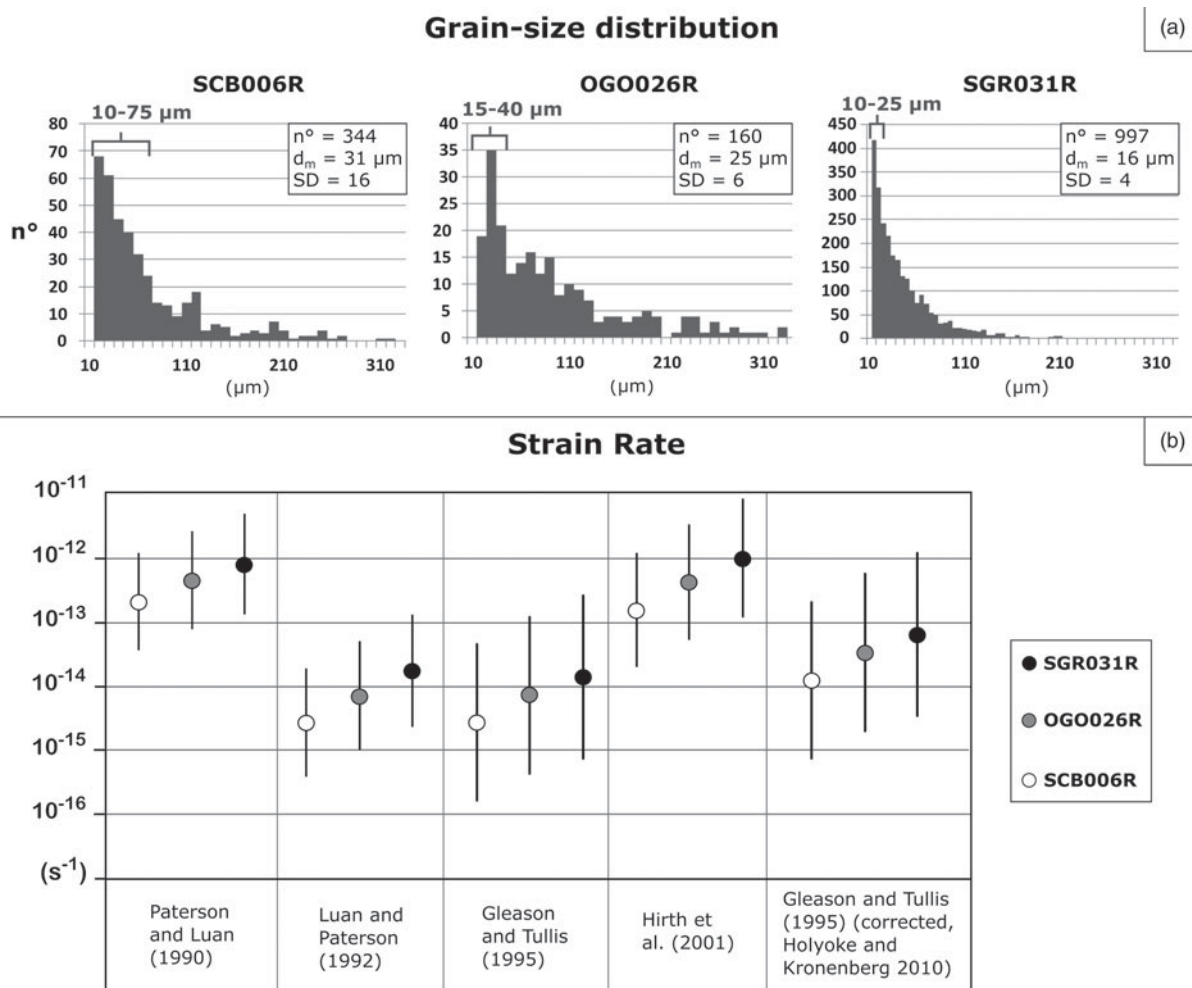


Fig. 12. (a) Quartz grain-size distributions for the selected sample. See Figure 6 for sample locations. The grain-size intervals used for palaeopiezometry have been picked out from the total distribution, selecting the D₂late new grains formed by SGR, which represent the finest population of grains for each sample. (b) Results of strain rate (s⁻¹) estimations from the analysed samples using the different quartz flow law calibrations in the dislocation creep regime. A consistent trend of increasing strain rates towards the N (i.e. from sample SCB006R to sample SGR031R) is evident.

5.b. Quartz deformation

The important role of quartz in governing the rheology of the analysed rocks is evidenced by the modal abundance of this phase. The modal estimations show a quartz percentage range of 24 to 81 % (Table 1), reaching the minimum abundance (Fig. 7) to be considered the strain-supporting phase in each specimen (~20 % according to Handy, 1990). A quartz-dominated rheology

allowed us to consider the CPO analysis, performed on quartz ribbons, reliable at the larger scale.

At fluid-present conditions and at geological strain rates (Law, 2014), microstructures in quartz related to GBM recrystallization are generally indicative of dislocation creep deformation under amphibolite-facies metamorphic conditions (Stipp *et al.* 2002a,b). The transition from GBM to SGR can be related to several factors:

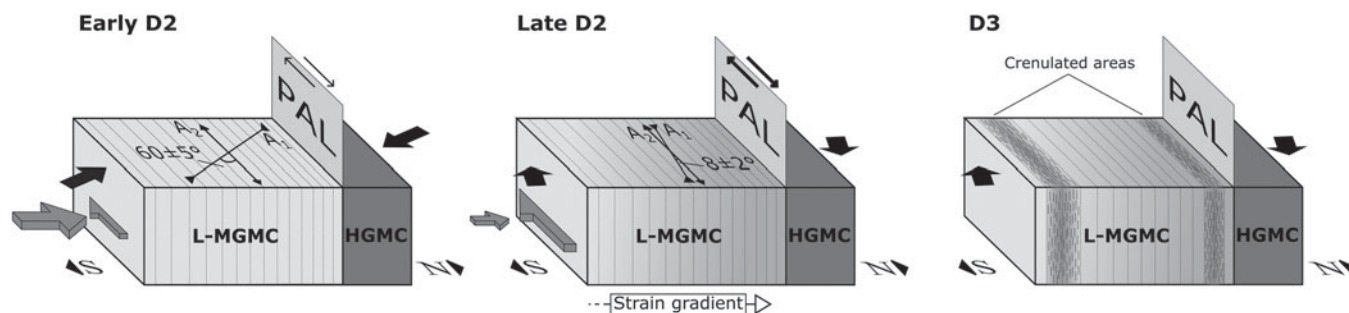


Fig. 13. Simplified reconstruction of the structural evolution of the L-MGMC during the transpressive tectonics linked to the PAL. The transpression developed in a pure shear dominated general flow during the D2_{early} and evolved into a simple shear dominated flow during the D2_{late}. The D2_{late} deformation is characterized by an increasing strain gradient moving towards the core of the PAL. During the D3 phase, the last deformation increments may have been accommodated by the development of crenulation cleavage, and related plunging upright folds. For the D2_{early} and the D2_{late} events the position and the angle between the flow apophyses (A_1 and A_2) has been inferred from the kinematic vorticity data. As the kinematic vorticity increases, the angle between the apophyses decreases.

a variation in deformation temperature, a decrease in water content or an increase in strain rate (Stipp *et al.* 2002a,b; Menegon *et al.* 2008, 2011; Law, 2014 and references therein). On the other hand, assuming no significant variations in water content and strain rate, SGR recrystallization (Fig. 5a–c) suggests a dislocation creep regime under a lower deformation temperature with respect to GBM (Stipp *et al.* 2002a,b; Passchier & Trouw, 2005; Law, 2014). The dextral sense of shear, testified to by the orientation of the oblique foliation, highlighted by quartz grains recrystallized by SGR fits well with the dominant sense of shear during the activity of the PAL. The syn-kinematic growth of retrograde assemblages, including chlorite along the C' planes (Fig. 4c, e), suggests a continuation of the PAL activity from higher to lower temperatures. This transition is testified to also by the quartz c -axis opening angle that points to lower temperatures compared to the peak conditions associated with the D2 (see Carosi & Palmeri, 2002; Di Vincenzo *et al.* 2004). For these reasons we infer that the superimposition of SGR is related mainly to a syn-shearing temperature decrease. In this framework, according to the structural and metamorphic evidence discussed above, a complex (and long-lasting) evolution of the D2 phase has been inferred. The D2 deformation phase is subdivided in two stages: an early D2_{early} stage associated with the thermal D2 peak, and a late D2_{late} stage as part of the retrograde exhumation path with decreasing temperatures. The variation in quartz dislocation creep regime from GBM to SGR is linked to a temperature decrease, and the acquisition of CPO data on the areas affected by SGR recrystallization allowed the constraining of the conditions of the D2_{late} deformation increments. The temperature of nearly 400 °C, derived from the c -axes opening angle, is consistent with the greenschist-facies metamorphism and suggests a thermal homogenization during the late stages of D2.

The kinematic vorticity analysis performed on recrystallized quartz aggregates resulted in high W_n values (0.91–1.00) indicative of a simple shear dominated flow (Fig. 11). Previous studies (Carosi & Palmeri, 2002; Carosi *et al.* 2005) pointed out a pure shear dominated flow in the same study area ($W_m = 0.30–0.70$), estimated using the stable porphyroclasts method (Passchier, 1987; Wallis *et al.* 1993; Xypolias, 2010). A possible explanation for these different results could be found in the different methods applied to the estimation of the kinematic vorticity values. It is necessary to take into account the different strain memory of the quartz recrystallization with respect to the porphyroclasts (Wallis, 1995; Xypolias, 2009, 2010). Carosi & Palmeri (2002) and Carosi *et al.* (2005) applied the stable porphyroclasts method using K-feldspar and plagioclase porphyroclasts, crystallized before the D2 phase and

experiencing a rigid-clast behaviour during the PAL shearing. Competency contrast could be responsible for strain partitioning (Goodwin & Tikoff, 2002), so that some minerals, such as, for example, K-feldspar, with a different viscosity than quartz, could partition different kinematic (coaxial versus non-coaxial) and rheological (brittle versus viscous) components of the bulk deformation. On the other hand, quartz microstructures and CPO have a shorter strain memory (Xypolias, 2009, 2010) and better record the late deformation increments, especially in our case study, where the later SGR recrystallization areas were selected for the EBSD analysis. From the comparison of the data acquired by the two different methods, likely related to different stages of the transpression, it is possible to better reconstruct the kinematic evolution of the PAL, which was dominated by pure shear during the early deformation stages and by simple shear in the late deformation increments (Fig. 13).

Other transpressive systems, showing a bulk non-coaxial deformation, with a deformation regime evolving from a pure shear dominated transpression to a simple shear dominated transpression, have been documented by Carreras *et al.* (2010).

5.c. Consideration of the exhumation mechanism

Shear zones are common features in deforming rocks and occur at all scales from the millimetre scale to the kilometre scale (Fossen & Cavalcante, 2017). Whereas most of the studies have focused on metre- to hectometre-scale shear zones, comparatively fewer studies are available for regional-scale shear zones and on the consequences on the P – T – t paths of the deformed rocks. In the Himalayas, a regional-scale (thrust-sense) shear zone running for more than 1000 km along-strike, the High Himalayan Discontinuity (Montomoli *et al.* 2013, 2015), affected the tectonic and metamorphic evolution of the metamorphic core of the belt for more than 10–15 Ma (Carosi *et al.* 2018).

Analogously, the PAL is an example of a (transpressive) crustal-scale shear zone that affected the inner portion of the Variscan Belt for several hundred kilometres (from Sardinia–Corsica and the Maures massif up to the External Massifs of the Alps: Corsini & Rolland, 2009; Simonetti *et al.* 2018 with references) for more than *c.* 20 Ma (Carosi *et al.* 2012; Simonetti *et al.* 2018), and it efficiently exhumed the deeper portions of the belt from medium-temperature up to low-temperature conditions, playing a primary role in the tectonic end-metamorphic evolution of the Variscan Belt. Considering the overall development of the PAL and its prosecution in the External Crystalline Massifs of the Alps, this first-order

shear zone is a major zone of weakness in the crust, and it allowed further localization of the deformation during the first stages of the Alpine cycle (Bergomi *et al.* 2017; Balleve *et al.* 2018).

The PAL has a sub-horizontal or gently plunging (L2) stretching lineation and sub-vertical foliation, and the exhumation could be expected to be driven by a nearly horizontal extrusion (e.g. Tikoff & Fossen, 1993; Schulmann *et al.* 2003; Iacopini *et al.* 2008). On the other hand, mylonite in a transpressive zone could be affected by vertical movement of the rock flow. This case, where pure and simple shear are active coevally during deformation, is typically related to a vertical stretching lineation during the whole deformation history or caused by the flipping of an originally shallowly plunging lineation to a vertical attitude (Tikoff & Fossen, 1993; Schulmann *et al.* 2003; Iacopini *et al.* 2008). However, in simple shear dominated transpression, in the case of vertical extrusion, horizontal lineation can be preserved (Iacopini *et al.* 2008). It is worth noting that in the study sector of the PAL, the kinematic flow was dominated by simple shear only during the latest D2 increments. The L2 is marked by feldspars, quartz and syn-D2_{early} porphyroblasts of garnet and staurolite. During the D2_{early} phase, the kinematic flow was in general shear condition with a sub-horizontally directed simple shear component (Carosi & Palmeri, 2002). A major component of pure shear is not compatible with the development of a horizontal lineation in the case of vertical flow, and for this reason the occurrence of a vertical extrusion during the whole duration of PAL activity is unlikely. Considering the high W_n value, close to simple shear, recorded for the D2_{late} phase, the horizontal lineation related to this phase could be developed in both horizontal or vertical extrusion regimes. The structural data relative to the D2 phase are compatible with two different hypotheses of tectonic evolution: (i) a constant horizontal or slightly oblique extrusion or (ii) a composite evolution with horizontal extrusion in the D2_{early} and vertical extrusion in the D2_{late} phases.

5.d. Strain partitioning during the late D2 stage

As previously mentioned, the superposition intensity of SGR (D2_{late}) microstructures over the older GBM (D2_{early}) fabric in quartz aggregates increases moving from south to north in the study area, reaching the highest intensity approaching the core of the PAL. Considering that the deformation temperature during D2_{late} was nearly homogeneous along the N–S study transect, as suggested by syn-kinematic minerals and opening angle thermometry, the increase in SGR intensity cannot be attributed to a (significant) temperature variation. On the contrary, petrofabric data suggest that the strain rate spatially increases moving to the north from $\sim 10^{-13} \text{ s}^{-1}$ to $\sim 10^{-12} \text{ s}^{-1}$ according to the Hirth *et al.* (2001) flow law (Fig. 12b). Thus, we can infer that strain rate variations played an important role in the microstructural evolution of quartz during SGR recrystallization in this area (Hobbs, 1985; Passchier & Trouw, 2005).

The grain-size palaeopiezometry and strain rate estimates, performed on the analysed samples, can be compared with other data available in the literature for the Sardinian Variscan Belt (e.g. Casini *et al.* 2010; Casini & Funedda, 2014; Montomoli *et al.* 2018). According to these authors, the strain rates increase moving from south to north, ranging from $\sim 10^{16} \text{ s}^{-1}$ to $\sim 10^{15} \text{ s}^{-1}$ in the Foreland Zone to $\sim 10^{15} \text{ s}^{-1}$ to $\sim 10^{13} \text{ s}^{-1}$ in the Nappe Zone and $\sim 10^{13} \text{ s}^{-1}$ to $\sim 10^{11} \text{ s}^{-1}$ in the Inner Zone.

The strain rate proposed in this work is closely comparable to the results obtained by Casini *et al.* (2010) in the same area of the orogen. These estimations also exceed the value of 10^{-14} s^{-1}

proposed as a typical geological strain rate (Pfiffner & Ramsay, 1982; Passchier & Trouw, 2005). Nevertheless, it is worthwhile to consider the discussion recently opened by Fagereng & Biggs (2019) where they postulate on the underestimation of 10^{-14} s^{-1} as a typical strain rate value.

6. Conclusions

Data from geological mapping and structural analysis, at different scales, allowed the constraint of the tectonic evolution of the northern sector of the Variscan Belt in Sardinia within the L–MGMC close to the PAL. The PAL is regarded as an orogen-parallel transpressional shear zone that drove the exhumation of the Sardinian metamorphic complexes. In the northern L–MGMC, the shearing event is represented by the D2 phase, which started to be active close to the metamorphic ‘peak’, under amphibolite-facies conditions (D2_{early}), and lasted up to greenschist-facies conditions during the D2_{late} event. The transpressive tectonics related to the PAL continued during the D3 phase under even shallower crustal conditions. The shift in metamorphic conditions caused strain partitioning along the mylonitic belt, giving rise to shear zone-parallel discontinuous domains characterized by the folding of S2 foliation (Fig. 13).

Quartz petrofabrics, together with microstructural data, suggest that the transition from D2_{early} to D2_{late} has been characterized by:

- (1) a nearly thermal homogenization at $\sim 400 \text{ }^\circ\text{C}$ where a shift in the dynamic recrystallization mechanisms in quartz aggregates, from GBM to SGR, is documented. The SGR overprinting microstructures are incipiently developed in the southern area and gradually become more pervasive moving into the northern area;
- (2) an increase in the simple shear component during deformation, ranging from pure shear to simple shear dominated transpression (Fig. 13).

Comparing the structural analysis data with the available kinematic vorticity estimates, based on different vorticity gauges, it is possible to infer that the PAL, in the study area, led to a tectonic evolution characterized by horizontal extrusion or, alternatively, by a horizontal extrusion occurring during the D2_{early} phase followed by a vertical extrusion coeval with the D2_{late} phase. With the present data it is not possible to verify the latter hypothesis and to clarify the kinematics of the late mylonitic flow of the PAL, and further investigations are needed.

The flow stresses and the strain rates suggest an increase in these two parameters moving closer to the core of the PAL. This variation is in agreement with the presence of the superimposition of the SGR recrystallization mechanism in quartz in the northern sector.

The new data support a framework in which a single long-lasting, crustal-scale shear zone, once formed at depth, is able to continue to localize deformation and to drive the exhumation of the inner portions of the belt towards lower P – T conditions. This shear zone, continuing in other portions of the Southern Variscan Belt, was active until the end of the Variscan Orogeny and acted as a weak zone reactivated during the later Alpine tectonics.

Acknowledgements. The staff at the Plymouth University Electron Microscopy Centre is thanked for support during EBSD analysis. Funding: PRIN 2015 (University of Torino: R. Carosi and C. Montomoli); funds Ricerca Locale University of Torino (ex-60%, R. Carosi and S. Iaccarino); PRA 20018_41 to C. Montomoli. Jorge Alonso-Henar and Eugenio Fazio are thanked for their careful reviews. We thank the editor, Prof. Lacombe for his very efficient handling of the paper.

References

- Alvarez W (1972) Rotation of the Corsica–Sardinia Microplate. *Nature* **235**, 103–5. doi: [10.1038/physci235103a0](https://doi.org/10.1038/physci235103a0).
- Balleve M, Manzotti P and Dal Piaz GV (2018) Pre-Alpine (Variscan) inheritance: a key for the location of the future Valais Basin (Western Alps). *Tectonics* **37**, 786–817. doi: [10.1002/2017TC004633](https://doi.org/10.1002/2017TC004633).
- Bergomi MA, Dal Piaz GV, Malusà MG, Monopoli B and Tunesi A (2017) The Grand St Bernard–Briançonnais nappe system and the Paleozoic inheritance of the Western Alps unraveled by zircon U–Pb dating. *Tectonics* **36**, 2950–72. doi: [10.1002/2017TC004621](https://doi.org/10.1002/2017TC004621).
- Behr WM and Platt JP (2011) A naturally constrained stress profile through the middle crust in an extensional terrane. *Earth Planetary Science Letters* **303**, 181–92. doi: [10.1016/j.epsl.2010.11.044](https://doi.org/10.1016/j.epsl.2010.11.044).
- Behr WM and Platt JP (2013) Rheological evolution of a Mediterranean subduction complex. *Journal of Structural Geology* **54**, 136–55. doi: [10.1016/j.jsg.2013.07.012](https://doi.org/10.1016/j.jsg.2013.07.012).
- Behr WM and Platt JP (2014) Brittle faults are weak, yet the ductile middle crust is strong: implications for lithospheric mechanics. *Geophysical Research Letters* **41**, 8067–75. doi: [10.1002/2014GL061349](https://doi.org/10.1002/2014GL061349).
- Boutonnet E, Leloup PH, Sassièr C, Gardien V and Ricard Y (2013) Ductile strain rate measurements document long-term strain localization in the continental crust. *Geology* **41**, 819–22. doi: [10.1130/G33723.1](https://doi.org/10.1130/G33723.1).
- Burchfiel BC, Zhiliang C, Hodges KV, Yuping L, Royden LH, Changrong D and Jiè X (1992) *The South Tibetan Detachment System, Himalayan Orogen: Extension Contemporaneous with and Parallel to Shortening in a Collisional Mountain Belt*. Boulder, Colorado: Geological Society of America, Special Paper no. 269.
- Cappelli B, Carmignani L, Castorina F, Di Pisa A, Oggiano G and Petrini R (1992) The correct title is “A Hercynian suture zone in Sardinia: geological and geochemical evidence”, Paleozoic orogenies in Europe. *Geodinamica Acta* **5**, 101–18. doi: [10.1080/09853111.1992.11105222](https://doi.org/10.1080/09853111.1992.11105222).
- Carmignani L, Carosi R, Di Pisa A, Gattiglio M, Musumeci G, Oggiano G and Pertusati PC (1994) The Hercynian Chain in Sardinia (Italy). *Geodinamica Acta* **7**, 31–47. doi: [10.1080/09853111.1994.11105257](https://doi.org/10.1080/09853111.1994.11105257).
- Carmignani L, Cocozza T, Ghezzi C, Pertusati PC and Ricci CA (1982) Lineamenti del basamento sardo. In *Guida alla Geologia del Paleozoico Sardo* (eds L Carmignani, T Cocozza, C Ghezzi, PC Pertusati and CA Ricci), pp. 11–23. Bologna: Guide Geologiche Regionali, Società Geologica Italiana.
- Carmignani L, Oggiano G, Barca S, Conti P, Salvadori I, Eltrudis A, Funedda A and Pasci S (2001) Geologia della Sardegna. Note illustrative della Carta Geologica della Sardegna a scala 1:200.000. *Memorie Descrittive della Carta Geologica d'Italia* **60**, 283.
- Carosi R, Cruciani G, Franceschelli M and Montomoli C (2015) The Variscan basement in Sardinia. 29th Himalaya–Karakoram–Tibet Workshop, Lucca, 5–8 September 2014. *Geological Field Trips* **7**, 1–118. doi: [10.3301/GFT.2015.03](https://doi.org/10.3301/GFT.2015.03).
- Carosi R, D’Addario E, Mammoliti E, Montomoli C and Simonetti M (2016) Geology of the northwestern portion of the Ferriere–Mollières Shear Zone, Argentera Massif, Italy. *Journal of Maps* **12**, 466–75. doi: [10.1080/17445647.2016.1243491](https://doi.org/10.1080/17445647.2016.1243491).
- Carosi R, Di Pisa A, Iacopini D, Montomoli C and Oggiano G (2004) The structural evolution of the Asinara island (NW Sardinia, Italy). *Geodinamica Acta* **17**, 309–29. doi: [10.3166/ga.17.309-329](https://doi.org/10.3166/ga.17.309-329).
- Carosi R, Frassi C and Montomoli C (2009) Deformation during exhumation of medium- and high-grade metamorphic rocks in the Variscan chain in northern Sardinia (Italy). *Geological Journal* **44**, 280–305. doi: [10.1002/gj.1137](https://doi.org/10.1002/gj.1137).
- Carosi R, Musumeci G and Pertusati PC (1991) Differences in the structural evolution of tectonic units in central-southern Sardinia. *Bollettino della Società Geologica Italiana* **110**, 543–51. doi: [10.1016/j.earsirev.2017.11.006](https://doi.org/10.1016/j.earsirev.2017.11.006).
- Carosi R, Frassi C, Iacopini D and Montomoli C (2005) Post collisional transpressive tectonics in northern Sardinia (Italy). *Journal of the Virtual Explorer* **19**. doi: [10.3809/jvirtex.2005.00118](https://doi.org/10.3809/jvirtex.2005.00118).
- Carosi R, Montomoli C and Iaccarino S (2018) 20 years of geological mapping of the metamorphic core across Central and Eastern Himalayas. *Earth–Science Reviews* **177**, 124–38.
- Carosi R, Montomoli C, Tiepolo M and Frassi C (2012) Geochronological constraints on post-collisional shear zones in the Variscides of Sardinia (Italy). *Terra Nova* **24**, 42–51. doi: [10.1111/j.1365-3121.2011.01035.x](https://doi.org/10.1111/j.1365-3121.2011.01035.x).
- Carosi R and Oggiano G (2002) Transpressional deformation in northwestern Sardinia (Italy): insights on the tectonic evolution of the Variscan belt. *Comptes Rendus Geoscience* **334**, 287–94. doi: [10.1016/S1631-0713\(02\)01740-6](https://doi.org/10.1016/S1631-0713(02)01740-6).
- Carosi R and Palmeri R (2002) Orogen-parallel tectonic transport in the Variscan belt of northeastern Sardinia (Italy): implications for the exhumation of medium-pressure metamorphic rocks. *Geological Magazine* **139**, 497–511. doi: [10.1017/S0016756802006763](https://doi.org/10.1017/S0016756802006763).
- Carosi R and Pertusati PC (1990) Evoluzione strutturale delle unità tettoniche erciniche nella Sardegna centro-meridionale. *Bollettino della Società Geologica Italiana* **109**, 325–35.
- Carreras J, Czeck DM, Druguet E and Hudleston PJ (2010) Structure and development of an anastomosing network of ductile shear zones. *Journal of Structural Geology* **32**, 656–66. doi: [10.1016/j.jsg.2010.03.013](https://doi.org/10.1016/j.jsg.2010.03.013).
- Casini L, Cuccuru S, Maino M, Oggiano G and Tiepolo M (2012) Emplacement of the Arzachena Pluton (Corsica–Sardinia Batholith) and the geodynamics of incoming Pangaea. *Tectonophysics* **544**, 31–49. doi: [10.1016/j.tecto.2012.03.028](https://doi.org/10.1016/j.tecto.2012.03.028).
- Casini L, Cuccuru S, Puccini A, Oggiano G and Rossi P (2015) Evolution of the Corsica–Sardinia Batholith and late-orogenic shearing of the Variscides. *Tectonophysics* **646**, 65–78.
- Casini L and Funedda A (2014) Potential of pressure solution for strain localization in the Baccu Locci Shear Zone (Sardinia, Italy). *Journal of Structural Geology* **66**, 188–204. doi: [10.1016/j.jsg.2014.05.016](https://doi.org/10.1016/j.jsg.2014.05.016).
- Casini L, Funedda A and Oggiano G (2010) A balanced foreland–hinterland deformation model for the Southern Variscan belt of Sardinia, Italy. *Geological Journal* **45**, 634–49. doi: [10.1002/gj.1208](https://doi.org/10.1002/gj.1208).
- Corsini M and Rolland Y (2009) Late evolution of the southern European Variscan belt: exhumation of the lower crust in a context of oblique convergence. *Comptes Rendus Geoscience* **341**, 214–23. doi: [10.1016/j.crte.2008.12.002](https://doi.org/10.1016/j.crte.2008.12.002).
- Cortesogno L, Gaggero L, Oggiano G and Paquette JL (2004) Different tectono-thermal evolutionary paths in eclogitic rocks from the axial zone of the Variscan chain in Sardinia (Italy) compared with the Ligurian Alps. *Ophioliti* **29**, 125–44. doi: [10.4454/Ophioliti.v29i2.210](https://doi.org/10.4454/Ophioliti.v29i2.210).
- Cruciani G, Franceschelli M, Massonne HJ, Carosi R and Montomoli C (2013) Pressure temperature and deformational evolution of high pressure metapelites from Variscan NE Sardinia, Italy. *Lithos* **175–176**, 272–84. doi: [10.1016/j.lithos.2013.05.001](https://doi.org/10.1016/j.lithos.2013.05.001).
- Cruciani G, Montomoli C, Carosi R, Franceschelli M and Puxeddu M (2015) Continental collision from two perspectives: a review of Variscan metamorphism and deformation in northern Sardinia. *Periodico di Mineralogia* **84**, 657–99. doi: [10.2451/2015PM0455](https://doi.org/10.2451/2015PM0455).
- Deino A, Gattacceca J, Rizzo R and Montanari A (2001) ⁴⁰Ar/³⁹Ar dating and paleomagnetism of the Miocene volcanic succession of Monte Furrù (Western Sardinia): implications for the rotation history of the Corsica–Sardinia Microplate. *Geophysical Research Letters* **28**, 3373–6. doi: [10.1029/2001GL012941](https://doi.org/10.1029/2001GL012941).
- Depine GV, Andronicos CL and Hollister LS (2011) Response of continental magmatic arcs to regional tectonic changes recorded by synorogenic plutons in the middle crust: an example from the Coast Mountains of British Columbia. *Journal of Structural Geology* **33**, 1089–104. doi: [10.1016/j.jsg.2011.03.012](https://doi.org/10.1016/j.jsg.2011.03.012).
- Di Pisa A, Oggiano G and Talarico F (1993) Post collisional tectono-metamorphic evolution in the axial zone of the Hercynian belt in Sardinia: the example from the Asinara Island. *Bulletin du Bureau de Recherches Géologiques et Minières* **219**, 216–17.
- Di Vincenzo G, Carosi R and Palmeri R (2004) The relationship between tectono-metamorphic evolution and argon isotope records in white mica: constraints from in situ ⁴⁰Ar–³⁹Ar laser analysis of the Variscan basement of Sardinia. *Journal of Petrology* **45**, 1013–43. doi: [10.1093/ptrology/egh002](https://doi.org/10.1093/ptrology/egh002).
- Elter FM, Musumeci G and Pertusati PC (1990) Late Hercynian shear zones in Sardinia. *Tectonophysics* **176**, 387–404. doi: [10.1016/0040-1951\(90\)90080-R](https://doi.org/10.1016/0040-1951(90)90080-R).
- Fagereng Å and Biggs J (2019) New perspectives on ‘geological strain rates’ calculated from both naturally deformed and actively deforming rocks. *Journal of Structural Geology* **125**, 100–10. doi: [10.1016/j.jsg.2018.10.004](https://doi.org/10.1016/j.jsg.2018.10.004).

- Faleiros FM, Moraes R, Pavan N and Campanha GAC** (2016) A new empirical calibration of the quartz *c*-axis fabric opening-angle deformation thermometer. *Tectonophysics* **671**, 173–82. doi: [10.1016/j.tecto.2016.01.014](https://doi.org/10.1016/j.tecto.2016.01.014).
- Fazio E, Ortolano G, Visalli R, Cirrincione R, Fiannacca P, Mengel K, Pezzino A and Punturo R** (2018) Strain rates of the syn-tectonic Symvolon pluton (Southern Rhodope Core Complex, Greece): an integrated approach combining quartz paleopiezometry, flow laws and PT pseudosections. *Italian Journal of Geosciences* **137**, 208–18. doi: [10.3301/IJG.2018.10](https://doi.org/10.3301/IJG.2018.10).
- Fazio E, Punturo R, Cirrincione R, Kern H, Pezzino A, Wenk HR, Goswami S and Mamtani MA** (2017) Quartz preferred orientation in naturally deformed mylonitic rocks (Montalto shear zone–Italy): a comparison of results by different techniques, their advantages and limitations. *International Journal of Earth Sciences* **106**, 2259–78. doi: [10.1007/s00531-016-1424-y](https://doi.org/10.1007/s00531-016-1424-y).
- Fossen H and Cavalcante GC** (2017) Shear zones – a review. *Earth-Science Reviews* **171**, 434–55.
- Fossen H and Tikoff B** (1998) Extended models of transpression and transtension, and application to tectonic settings. In *Continental Transpressional and Transtensional Tectonics* (eds RE Holdsworth, RA Strachan and JF Dewey), pp. 15–33. Geological Society of London, Special Publication no. 135. doi: [10.1144/GSL.SP.1998.135.01.02](https://doi.org/10.1144/GSL.SP.1998.135.01.02).
- Franceschelli M, Battaglia S, Cruciani G, Pasci S and Puxeddu M** (2017) Very low-temperature metamorphism in Ordovician metasedimentary rocks above and below the Sardinian unconformity, SW Sardinia, Italy. *International Journal of Earth Science* **106**, 531–48. doi: [10.1007/s00531-016-1370-8](https://doi.org/10.1007/s00531-016-1370-8).
- Franceschelli M, Memmi I, Pannuti F and Ricci CA** (1989) Diachronous metamorphic equilibria in the Hercynian basement of northern Sardinia, Italy. In *Evolution of Metamorphic Belts* (eds JS Daly, RA Cliff and BWD Yardley), pp. 371–5. Geological Society of London, Special Publication no. 43. doi: [10.1144/GSL.SP.1989.043.01.33](https://doi.org/10.1144/GSL.SP.1989.043.01.33).
- Franceschelli M, Memmi I and Ricci CA** (1982) Zoneografia metamorfica della Sardegna settentrionale. In *Guida alla Geologia del Paleozoico Sardo* (eds L Carmignani, T Cocozza, C Ghezzi, PC Pertusati and CA Ricci), pp. 137–49. Bologna: Guide Geologiche Regionali, Società Geologica Italiana.
- Franceschelli M, Puxeddu M, Cruciani G, Dini A and Loi M** (2005) Layered amphibolite sequence in NE Sardinia, Italy: remnant of a pre-Variscan mafic silicic layered intrusion? *Contributions to Mineralogy Petrology* **149**, 164–80. doi: [10.1007/s00410-004-0642-7](https://doi.org/10.1007/s00410-004-0642-7).
- Frassi C, Carosi R, Montomoli C and Law RD** (2009) Kinematics and vorticity of flow associated with post-collisional oblique transpression in the Variscan Inner Zone of northern Sardinia (Italy). *Journal of Structural Geology* **31**, 1458–71. doi: [10.1016/j.jsg.2009.10.001](https://doi.org/10.1016/j.jsg.2009.10.001).
- Gattacceca J** (2001) Cinématique du bassin Liguro Provençal entre 30 et 12 Ma: implications géodynamiques. *Mémoires des sciences de la Terre. Ecole des mines de Paris* **41**, 299.
- Gébelin A, Rogera F and Brunel M** (2009) Syntectonic crustal melting and high-grade metamorphism in a transpressional regime, Variscan Massif Central, France. *Tectonophysics* **477**, 229–43. doi: [10.1016/j.tecto.2009.03.022](https://doi.org/10.1016/j.tecto.2009.03.022).
- Ghezzi C, Memmi I and Ricci CA** (1979) Un evento granulitico nella Sardegna nord-orientale. *Memorie della Società Geologica Italiana* **20**, 23–38.
- Giacomini F, Bomparola RM and Ghezzi C** (2005). Petrology and geochronology of metabasites with eclogite facies relics from NE Sardinia: constraints for the Palaeozoic evolution of Southern Europe. *Lithos* **82**, 221–48.
- Giacomini F, Bomparola RM, Ghezzi C and Guldbransen H** (2006) The geodynamic evolution of the Southern European Variscides: constraints from the U/Pb geochronology and geochemistry of the lower Palaeozoic magmatic–sedimentary sequences of Sardinia (Italy). *Contributions to Mineralogy Petrology* **152**, 19. doi: [10.1007/s00410-006-0092-5](https://doi.org/10.1007/s00410-006-0092-5).
- Gleason GC and Tullis J** (1995) A flow law for dislocation creep of quartz aggregates determined with the molten salt cell. *Tectonophysics* **247**, 1–23. doi: [10.1016/0040-1951\(95\)00011-B](https://doi.org/10.1016/0040-1951(95)00011-B).
- Goodwin LB and Tikoff B** (2002) Competency contrast, kinematics and the development of foliations and lineations in the crust. *Journal of Structural Geology* **24**, 1065–85. doi: [10.1016/S01981-8141\(01\)00092-x](https://doi.org/10.1016/S01981-8141(01)00092-x).
- Goscombe B, Gray D and Hand M** (2005) Extrusional tectonics in the core of a transpressional orogen; the Kaoko Belt, Namibia. *Journal of Petrology* **46**, 1203–41. doi: [10.1093/petrology/egi014](https://doi.org/10.1093/petrology/egi014).
- Goscombe B, Hand M, Gray D and Mawby J** (2003) The metamorphic architecture of a transpressional orogen: the Kaoko Belt, Namibia. *Journal of Petrology* **44**, 679–711. doi: [10.1093/petrology/44.4.679](https://doi.org/10.1093/petrology/44.4.679).
- Handy MR** (1990) The solid-state flow of polymineralic rocks. *Journal of Geophysical Research: Solid Earth* **95**, 8647–61. doi: [10.1029/JB095iB06p08647](https://doi.org/10.1029/JB095iB06p08647).
- Helbing H and Tiepolo M** (2005) Age determination of Ordovician magmatism in NE Sardinia and its bearing on Variscan basement evolution. *Journal of the Geological Society, London* **162**, 689–700. doi: [10.1144/0016-764904-103](https://doi.org/10.1144/0016-764904-103).
- Hirth G, Teyssier C and Dunlap WJ** (2001) An evaluation of quartzite flow laws based on comparisons between experimentally and naturally deformed rocks. *International Journal of Earth Science* **90**, 77–87. doi: [10.1007/s005310000152](https://doi.org/10.1007/s005310000152).
- Hobbs BE** (1985) The geological significance of microfabric analysis. In *Preferred Orientation in Deformed Metals and Rocks* (ed. HR Wenk), pp. 463–84. New York: Academic Press. doi: [10.1016/b978-0-12-744020-0.50027-4](https://doi.org/10.1016/b978-0-12-744020-0.50027-4).
- Holyoke CW and Kronenberg AK** (2010) Accurate differential stress measurement using the molten salt cell and solid salt assemblies in the Griggs apparatus with applications to strength, piezometers and rheology. *Tectonophysics* **494**, 17–31. doi: [10.1016/j.tecto.2010.08.001](https://doi.org/10.1016/j.tecto.2010.08.001).
- Hunter NJ R, Weinberg RF, Wilson CJ L and Law RD** (2018) A new technique for quantifying symmetry and opening angles in quartz *c*-axis pole figures: implications for interpreting the kinematic and thermal properties of rocks. *Journal of Structural Geology* **112**, 1–6. doi: [10.1016/j.jsg.2018.04.006](https://doi.org/10.1016/j.jsg.2018.04.006).
- Iacopini D, Carosi R, Montomoli C and Passchier CW** (2008) Strain analysis and vorticity of flow in the Northern Sardinian Variscan belt: recognition of a partitioned oblique deformation event. *Tectonophysics* **446**, 77–96. doi: [10.1016/j.tecto.2007.10.002](https://doi.org/10.1016/j.tecto.2007.10.002).
- Kruhl JH** (1998) Reply: prism- and basal-plane parallel subgrain boundaries in quartz: a microstructural geothermobarometer. *Journal of Metamorphic Geology* **16**, 142–6. doi: [10.1046/j.1525-1314.1996.00413.x](https://doi.org/10.1046/j.1525-1314.1996.00413.x).
- Law RD** (1990) Crystallographic fabrics: a selective review of their applications to research in structural geology. In *Deformation Mechanisms, Rheology and Tectonics* (eds RJ Knipe and EH Rutter), pp. 335–52. Geological Society of London, Special Publication no. 54. doi: [10.1144/GSL.SP.1990.054.01.30](https://doi.org/10.1144/GSL.SP.1990.054.01.30).
- Law RD** (2014) Deformation thermometry based on quartz *c*-axis fabrics and recrystallization micro structures: a review. *Journal of Structural Geology* **66**, 129–61. doi: [10.1016/j.jsg.2014.05.023](https://doi.org/10.1016/j.jsg.2014.05.023).
- Law RD, Jessup MJ, Searle MP, Francis MK, Waters DJ and Cottle JM** (2011) Telescoping of isotherms beneath the South Tibetan detachment system, Mount Everest Massif. *Journal of Structural Geology* **33**, 1569–94. doi: [10.1016/j.jsg.2011.09.004](https://doi.org/10.1016/j.jsg.2011.09.004).
- Law RD, Mainprice D, Casey M, Lloyd GE, Knipe RJ, Cook B and Thigpen JR** (2010) Moine thrust zone mylonites at the Stack of Glencoul: I – microstructures, strain and influence of recrystallization on quartz crystal fabric development. In *Continental Tectonics and Mountain Building: The Legacy of Peach and Horne* (eds RD Law, RWH Butler, RE Holdsworth, M Krabbendam and RA Strachan), pp. 543–77. Geological Society of London, Special Publication no. 335. doi: [10.1144/SP335.23](https://doi.org/10.1144/SP335.23).
- Law RD, Searle MP and Simpson RL** (2004) Strain, deformation temperatures and vorticity of flow at the top of the Greater Himalayan Slab, Everest Massif, Tibet. *Journal of the Geological Society, London* **161**, 305–20. doi: [10.1144/0016-764903-047](https://doi.org/10.1144/0016-764903-047).
- Law RD, Stahr Iii DW, Francis MK, Ashley KT, Grasemann B and Ahmad T** (2013) Deformation temperatures and flow vorticities near the base of the Greater Himalayan Series, Sutlej Valley and Shimla Klippe, NW India. *Journal of Structural Geology* **54**, 21–53. doi: [10.1016/j.jsg.2013.05.009](https://doi.org/10.1016/j.jsg.2013.05.009).
- Lister GS and Hobbs BE** (1980) The simulation of fabric development during plastic deformation and its application to quartzite: the influence of deformation history. *Journal of Structural Geology* **2**, 355–71. doi: [10.1016/0191-8141\(80\)90023-1](https://doi.org/10.1016/0191-8141(80)90023-1).

- Luan FC and Paterson MS** (1992) Preparation and deformation of synthetic aggregates of quartz. *Geophysical Research Letters* **97**, 301–20. doi: [10.1029/91JB01748](https://doi.org/10.1029/91JB01748).
- Macera P, Conticelli S, Del Moro A, Di Pisa A, Oggiano G and Squadrone A** (1989) Geochemistry and Rb–Sr age of syntectonic peraluminous granites of Western Gallura, northern Sardinia: constraints on their genesis. *Periodico di Mineralogia* **58**, 25–43.
- Matte P** (1986) Tectonics and plate tectonics model for the Variscan belt of Europe. *Tectonophysics* **126**, 329–74. doi: [10.1016/0040-1951\(86\)90237-4](https://doi.org/10.1016/0040-1951(86)90237-4).
- Matte P, Lancelot J and Mattauer M** (1998) La zone axiale hercynienne de la Montagne Noire n'ets pas "metamorphic core complex" extensif mais un anticlinal post-nappe à coeur anatectique. *Geodinamica Acta* **11**, 13–22. doi: [10.1016/S0985-3111\(98\)80025-9](https://doi.org/10.1016/S0985-3111(98)80025-9).
- Menegon L, Nasipuri P, Stünitz H, Behrens H and Ravna E** (2011) Dry and strong quartz during deformation of the lower crust in the presence of melt. *Journal of Geophysical Research* **116**. doi: [10.1029/2011JB008371](https://doi.org/10.1029/2011JB008371).
- Menegon L, Pennacchioni G, Heilbronner R and Pittarello L** (2008) Evolution of quartz microstructure and c-axis crystallographic preferred orientation within ductilely deformed granitoids (Arolla Unit, Western Alps). *Journal of Structural Geology* **30**, 1332–47. doi: [10.1016/j.jsg.2008.07.007](https://doi.org/10.1016/j.jsg.2008.07.007).
- Miller C, Sassi FP and Armari G** (1976) On the occurrence of altered eclogitic rocks in northeastern Sardinia and their implication. *Neues Jahrbuch für Geologie und Palaontologie* **11**, 683–9.
- Montigny R, Edel JB and Thuizat R** (1981) Oligo-Miocene rotation of Sardinia: K–Ar ages and paleomagnetic data of Tertiary volcanics. *Earth and Planetary Science Letters* **54**, 261–71. doi: [10.1016/0012-821X\(81\)90009-1](https://doi.org/10.1016/0012-821X(81)90009-1).
- Montomoli C, Carosi R and Iaccarino S** (2015) Tectonometamorphic discontinuities in the Greater Himalayan Sequence: a local or a regional feature? In *Tectonics of the Himalaya* (eds S Mukherjee, R Carosi, PA van der Beek, BK Mukherjee and DM Robinson), pp. 25–41. Geological Society of London, Special Publication no. 412. doi: [10.1144/SP412.3](https://doi.org/10.1144/SP412.3).
- Montomoli C, Iaccarino S, Carosi R, Langone A and Visonà D** (2013) Tectonometamorphic discontinuities within the Greater Himalayan Sequence in Western Nepal (Central Himalaya): insights on the exhumation of crystalline rocks. *Tectonophysics* **608**, 1349–70. doi: [10.1016/j.tecto.2013.06.006](https://doi.org/10.1016/j.tecto.2013.06.006).
- Montomoli C, Iaccarino S, Simonetti M, Lezzerini M and Carosi R** (2018) Structural setting, kinematics and metamorphism in a km-scale shear zone in the Inner Nappes of Sardinia (Italy). *Italian Journal of Geoscience* **137**, 294–310. doi: [10.3301/IJG.2018.16](https://doi.org/10.3301/IJG.2018.16).
- Morgan SS and Law RD** (2004) Unusual transition in quartzite dislocation creep regimes and crystal slip systems in the aureole of the Eureka Valley–Joshua Flat–Beer Creek pluton, California: a case for anhydrous conditions created by decarbonation reactions. *Tectonophysics* **384**, 209–31. doi: [10.1016/j.tecto.2004.03.016](https://doi.org/10.1016/j.tecto.2004.03.016).
- Oggiano G and Di Pisa A** (1992) Geologia della catena ercinica in Sardegna – Zona Assiale. In *Struttura della Catena Ercinica in Sardegna: Guida alla Escursione sul Basamento Paleozoico* (ed. L Carmignani) pp. 148–77. Siena: Centrooffset.
- Ortolano G, Fazio E, Visalli R, Alsop GI, Pagano M and Cirrincione R** 2020. Quantitative microstructural analysis of mylonites formed during alpine tectonics in the Western Mediterranean realm. *Journal of Structural Geology* **131**, 1–14. doi: [10.1016/j.jsg.2019.103956](https://doi.org/10.1016/j.jsg.2019.103956).
- Palmeri R, Fanning M, Franceschelli M, Memmi I and Ricci CA** (2004) SHRIMP dating of zircons in eclogite from the Variscan basement in north-eastern Sardinia (Italy). *Neues Jahrbuch für Mineralogie Monatshefte* **6**, 275–88. doi: [10.1127/0028-3649/2004/2004-0275](https://doi.org/10.1127/0028-3649/2004/2004-0275).
- Passchier CW** (1987) Stable positions of rigid objects in non-coaxial flow—a study in vorticity analysis. *Journal of Structural Geology* **9**, 679–90. doi: [10.1016/0191-8141\(87\)90152-0](https://doi.org/10.1016/0191-8141(87)90152-0).
- Passchier CW and Trouw RA J** (2005) *Microtectonics*. Berlin: Springer. doi: [10.1007/3-540-29359-0](https://doi.org/10.1007/3-540-29359-0).
- Paterson MS and Luan FC** (1990) Quartzite rheology under geological conditions. In *Deformation Mechanisms, Rheology and Tectonics* (eds RJ Knipe and EH Rutter), pp. 299–307. Geological Society of London, Special Publication no. 54. doi: [10.1144/GSL.SP.1990.054.01.26](https://doi.org/10.1144/GSL.SP.1990.054.01.26).
- Pfiffner OA and Ramsay JG** (1982) Constraints on geological strain rates: arguments from finite strain states of naturally deformed rocks. *Journal of Geophysical Research* **87**, 311–21. doi: [10.1029/JB087iB01p00311](https://doi.org/10.1029/JB087iB01p00311).
- Ramsay JG** (1967) *Folding and Fracturing of Rocks*. New York: McGraw-Hill. doi: [10.1126/science.160.3826.410](https://doi.org/10.1126/science.160.3826.410).
- Sanderson DJ and Marchini WR D** (1984) Transpression. *Journal of Structural Geology* **6**, 449–58. doi: [10.1016/0191-8141\(84\)90058-0](https://doi.org/10.1016/0191-8141(84)90058-0).
- Schmid SM and Casey M** (1986) Complete fabric analysis of some commonly observed quartz c-axis patterns. In *Mineral and Rock Deformation: Laboratory Studies* (eds BE Hobbs and HC Heard), pp. 263–86. American Geophysical Union, Geophysical Monograph vol. 36. Washington, DC. doi: [10.1029/GM036p0263](https://doi.org/10.1029/GM036p0263).
- Schneider J, Corsini M, Reverso-Peila A and Lardeaux JM** (2014) Thermal and mechanical evolution of an orogenic wedge during Variscan collision: an example in the Maures-Tanneron Massif (SE France). In *The Variscan Orogeny: Extent, Timescale and the Formation of the European Crust* (eds K Schulmann, JR Martínez Catalán, JM Lardeaux, V Janoušek and G Oggiano), pp. 313–31. Geological Society of London, Special Publication no. 405. doi: [10.1144/SP405.4](https://doi.org/10.1144/SP405.4).
- Schulmann K, Thompson AB, Lexa O and Ježek, J** (2003) Strain distribution and fabric development modeled in active and ancient transpressive zones. *Journal of Geophysical Research* **108**, 6–15. doi: [10.1029/2001JB000632](https://doi.org/10.1029/2001JB000632).
- Searle MP, Law RD, Godin L, Larson KP, Streule MJ, Cottle JM and Jessup MJ** (2008) Defining the Himalayan main central thrust in Nepal. *Journal of the Geological Society, London* **165**, 523–34. doi: [10.1144/0016-76492007-081](https://doi.org/10.1144/0016-76492007-081).
- Simonetti M, Carosi R, Montomoli C, Langone A, D'Addario E and Mammoliti E** (2018) Kinematic and geochronological constraints on shear deformation in the Ferriere-Mollières shear zone (Argentera-Mercantour Massif, Western Alps): implications for the evolution of the Southern European Variscan belt. *International Journal of Earth Sciences* **107**, 2163–89. doi: [10.1007/s00531-018-1593-y](https://doi.org/10.1007/s00531-018-1593-y).
- Stipp M, Stünitz H, Heilbronner R and Schmid SM** (2002a) Dynamic recrystallization of quartz: correlation between natural and experimental conditions. In *Deformation Mechanisms, Rheology and Tectonics: Current Status and Future Perspectives* (eds S De Meer, MR Drury, JHP De Bresser and GM Pennock), pp. 171–90. Geological Society of London, Special Publication no. 200. doi: [10.1144/GSL.SP.2001.200.01.11](https://doi.org/10.1144/GSL.SP.2001.200.01.11).
- Stipp M, Stünitz H, Heilbronner R and Schmid SM** (2002b) The eastern Tonale fault zone: a “natural laboratory” for crystal plastic deformation of quartz over a temperature range from 250 to 700°C. *Journal of Structural Geology* **24**, 1861–84. doi: [10.1016/S0191-8141\(02\)00035-4](https://doi.org/10.1016/S0191-8141(02)00035-4).
- Stipp M and Tullis J** (2003) The recrystallized grain size piezometer for quartz. *Geophysical Research Letters* **30**, 20–88. doi: [10.1029/2003GL018444](https://doi.org/10.1029/2003GL018444).
- ten Grotenhuis SM, Trouw RAJ and Passchier CW** (2003) Evolution of mica fish in mylonitic rocks. *Tectonophysics* **372**, 1–21. doi: [10.1016/S0040-1951\(03\)00231-2](https://doi.org/10.1016/S0040-1951(03)00231-2).
- Thompson AB, Schulmann K and Jezek J** (1997) Thermal evolution and exhumation in obliquely convergent (transpressive) orogens. *Tectonophysics* **280**, 171–84. doi: [10.1016/S0040-1951\(97\)00144-3](https://doi.org/10.1016/S0040-1951(97)00144-3).
- Tikoff B and Fossen H** (1993) Simultaneous pure and simple shear: the unifying deformation matrix. *Tectonophysics* **217**, 267–83. doi: [10.1016/0040-1951\(93\)90010-h](https://doi.org/10.1016/0040-1951(93)90010-h).
- Tikoff B and Teyssier C** (1994) Strain modelling of displacement-field partitioning in transpressional orogens. *Journal of Structural Geology* **16**, 1575–88. doi: [10.1016/0191-8141\(94\)90034-5](https://doi.org/10.1016/0191-8141(94)90034-5).
- Tödheide K** (1972) Water at high temperatures and pressures. In *The Physics and Physical Chemistry of Water. Water (A Comprehensive Treatise)*, vol. 1. (ed. F Franks), pp. 463–514. Boston, MA: Springer. doi: [10.1007/978-1-4684-8334-5_13](https://doi.org/10.1007/978-1-4684-8334-5_13).
- Toy VG, Prior DJ and Norris RJ** (2008) Quartz fabrics in the Alpine Fault mylonites: influence of pre-existing preferred orientations on fabric development during progressive uplift. *Journal of Structural Geology* **30**, 602–21. doi: [10.1016/j.jsg.2008.01.001](https://doi.org/10.1016/j.jsg.2008.01.001).
- Turrillot P, Augier R, Monié P and Faure M** (2011) Late orogenic exhumation of the Variscan highgrade units (South Armorican Domain, western France), combined Structural and ⁴⁰Ar/³⁹Ar constraints. *Tectonics* **30**. doi: [10.1029/2010TC002788](https://doi.org/10.1029/2010TC002788).

- Twiss RJ** (1977) Theory and applicability of a recrystallized grain size paleopiezometer. In *Stress in the Earth* (ed. M Wyss), pp. 227–44. Contributions to Current Research in Geophysics (CCRG). Basel: Birkhäuser. doi: [10.1007/978-3-0348-5745-1_13](https://doi.org/10.1007/978-3-0348-5745-1_13).
- Wallis SR** (1995) Vorticity analysis and recognition of ductile extension in the Sambagawa belt, SW Japan. *Journal of Structural Geology* **17**, 1077–93. doi: [10.1016/0191-8141\(95\)00005-X](https://doi.org/10.1016/0191-8141(95)00005-X).
- Wallis SR, Platt JP and Knott SD** (1993) Recognition of syn-convergence extension in accretionary wedges with examples from the Calabrian Arc and the Eastern Alps. *American Journal of Science* **293**, 463–94. doi: [10.2475/ajs.293.5.463](https://doi.org/10.2475/ajs.293.5.463).
- Xypolias P** (2009) Some new aspects of kinematic vorticity analysis in naturally deformed quartzites. *Journal of Structural Geology* **31**, 3–10. doi: [10.1016/j.jsg.2008.09.009](https://doi.org/10.1016/j.jsg.2008.09.009).
- Xypolias P** (2010) Vorticity analysis in shear zones: a review of methods and applications. *Journal of Structural Geology* **32**, 2072–92. doi: [10.1016/j.jsg.2010.08.009](https://doi.org/10.1016/j.jsg.2010.08.009).
- Xypolias P and Koukouvelas IK** (2001) Kinematic vorticity and strain rate patterns associated with ductile extrusion in the Chelmos shear Zone (External Hellenides, Greece). *Tectonophysics* **338**, 59–77. doi: [10.1016/S0040-1951\(01\)00125-1](https://doi.org/10.1016/S0040-1951(01)00125-1)